UNIVERSITÄT PADERBORN
Die Universität der Informationsgesellschaft

FAKULTÄT FÜR
ELEKTROTECHNIK,
INFORMATIK UND
MATHEMATIK

Implementation and Simulation Study of Coherent Optical Orthogonal Frequency-Division Multiplexing Systems

Von der Fakultät für Elektrotechnik, Informatik und Mathematik
der Universität Paderborn

zur Erlangung des akademischen Grades

Doktor der Ingenieurwissenschaften (Dr.-Ing.)

genehmigte Dissertation

von

M.Sc. Omar H. A. Jan

Erster Gutachter: Prof. Dr.-Ing. Reinhold Noé
Zweiter Gutachter: Prof. Dr.-Ing. Reinhold Häb-Umbach

Tag der mündlichen Prüfung: 10.06.2015

Paderborn 2015

Diss. EIM-E/298

Abstract

In recent years, the demand for Internet traffic has increased due to the wide deployment of high-speed web services over the Internet, such as video streaming through YouTube and traditional TV channels. This increase in the demand requires infrastructure network capacity to be increased, particularly in the optical domain. In particular, the spectral efficiency must be enhanced to satisfy the demand for high capacity. One way to enhance the spectral efficiency is to use the orthogonal frequency division multiplex (OFDM) modulation format for optical communication.

In this dissertation, a simulation study of coherent-optical OFDM (CO-OFDM) systems has been conducted. Fiber nonlinearities are the main limitation for long-haul CO-OFDM transmission. A second limitation is the high impact of laser phase noise (LPN) imposed by the large linewidth of low-cost distributed feedback (DFB) lasers. Furthermore, high-order constellations (16-QAM) combined with large OFDM symbols (1024-point inverse fast Fourier transform (IFFT)/fast Fourier transform (FFT)) increase the penalty of such impairments. The larger OFDM symbols reduce the overhead of the cyclic prefix, and high-order constellations provide high spectral efficiency. Therefore, several combination techniques have been proposed and studied to alleviate the effect of fiber nonlinearities for long-haul CO-OFDM systems and of LPN for CO-OFDM systems that use DFB lasers.

The experimental demonstration of CO-OFDM systems has been achieved in this dissertation using off-line processing, where the received data are stored by a sampling oscilloscope and then evaluated using MATLAB. First, the experimental setups of a homodyne CO-OFDM system and a self-homodyne CO-OFDM system have been carried out with DFB lasers. Two-stage LPN mitigation is then proposed, for which the experimental results exhibit an improvement in the bit error ratio (BER). Second, some experiments have been carried out to investigate the

impact of LPN on DFT-spread CO-OFDM systems. Furthermore, a new spectral shaping technique for DFT-spread OFDM has been experimentally studied over a distance of approximately 347 km.

Zusammenfassung

Die Nachfrage nach Datenverkehr im Internet ist in letzter Zeit stark angewachsen wegen des Ausbaus von Diensten wie YouTube, Videoübertragung, Fernsehen über Internet und Ähnliches. Das erfordert eine Steigerung der Netzkapazität, insbesondere im optischen Bereich. Insbesondere wird eine Vergrösserung der spektralen Effizienz benötigt, um die Nachfrage an hoher Übertragungskapazität zu decken. Ein eleganter Ansatz ist die Erhöhung der spektralen Effizienz durch Verwendung von orthogonalem Frequenzmultiplexverfahren (OFDM) bei der optischen Übertragung.

Als Erstes wurden in dieser Dissertation CO-OFDM-Systeme anhand von Simulationen untersucht. Für Langstreckenübertragung mit OFDM sind Nichtlinearitäten des Lichtwellenleiters das begrenzende Moment. Ein zweiter ebenfalls begrenzender Effekt ist die starke Auswirkung des Phasenrauschens aufgrund der grossen Linienbreite von kostengünstigeren DFB-Lasern. Darüber hinaus führen Symbolkonstellationen höherer Ordnung (16-QAM) in Kombination mit langen OFDM-Symbolen (1024-Punkt IFFT/FFT) zu hohen Beeinträchtigungen aufgrund dieser Merkmale. Andererseits erlauben lange OFDM-Symbole eine Reduktion des zylischen Präfixes, und Symbolkonstellationen höherer Ordnung bedeuten eine hohe spektrale Effizienz. Um die Auswirkungen von Fasernichtlinearitäten und Laser-Phasenrauschen zu mildern wurden verschiedene Kombinationstechniken vorgeschlagen und an Langstreckensystemen mit CO-OFDM untersucht bei Verwendung von DFB-Lasern.

Als Zweites wurden CO-OFDM-Systeme experimentell untersucht mit Homodyn-Detektion, wobei die Signale im Oszilloskop gespeichert und anschliessend offline mit MATLAB verarbeitet wurden. Zuerst wurden in dieser Dissertation Experimente mit einem Homodyn-CO-OFDM-System und einem Selbst-Homodyn-Detektion ausgeführt mit DFB-Lasern. Eine zweistufige Methode zur Abschwächung

der Auswirkung des Phasenrauschens des Lasers wurde vorgeschlagen, und die Experimente zeigten eine Verbesserung der BER. Als zweites wurde die Auswirkung des Laser-Phasenrauschens auf CO-OFDM-Systeme mit unterteilter DFT experimentell untersucht. Ein neue spektrale Fensterung ebenfalls für CO-OFDM-Systeme mit unterteilter DFT wurde experimentell untersucht für eine Strecke von ca. 347 km.

Acknowledgements

First, I owe a debt of gratitude to Prof. Dr.-Ing. Reinhold Noé for his support during my work toward the Ph.D. degree since I joined the Optical Communication and High-Frequency Engineering group in January 2011. I wish to express my sincere thanks to Dr. David Sandel, Mr. Christian Wördehoff from CITEC at Bielefeld University and Mr. Horst Wernz from Ericsson GmbH for their help and support in the experimental setup.

I would also like to thank all of my research colleagues and technical staff at the ONT group for their collaboration in producing this work, and my sincere thanks goes to Prof. Dr.-Ing. Reinhold Häb-Umbach for his support.

I am particularly grateful to my parents for encouraging me to pursue doctoral research.

A special thanks goes to my lovely wife for her love and compassion and to my charming daughters, who make my life wonderful.

Contents

Abstract i

Zusammenfassung iii

Acknowledgements v

List of Figures ix

Abbreviations xi

Symbols xiv

1 Introduction 1
- 1.1 Overview . . . 1
- 1.2 Motivation . . . 2
- 1.3 Publications . . . 4
  - 1.3.1 Journal Papers . . . 4
  - 1.3.2 Conference Papers . . . 4

2 Fundamentals of CO-OFDM 8
- 2.1 Principles of OFDM . . . 8
  - 2.1.1 Principle of Orthogonality . . . 9
  - 2.1.2 Discrete and Fast Fourier Transform for OFDM . . . 10
  - 2.1.3 Cyclic Prefix (CP) . . . 11
  - 2.1.4 Spectral Efficiency (SE) . . . 12
- 2.2 DSP Algorithms for CO-OFDM System . . . 13
  - 2.2.1 Window Synchronization . . . 13
  - 2.2.2 Carrier Frequency Offset (CFO) . . . 14
  - 2.2.3 Channel Estimation and Correction . . . 16
  - 2.2.4 Laser Phase Noise (LPN) . . . 18
  - 2.2.5 Peak-to-Average Power Ratio (PAPR) . . . 19

3 Simulation Study of CO-OFDM Systems **21**
3.1 Study of Fiber Nonlinearities in CO-OFDM Systems 21
3.1.1 RF-pilot (RFP) method for XPM mitigation 22
3.1.1.1 Concept of the RF-pilot (RFP) method 22
3.1.1.2 Simulation Setup 22
3.1.1.3 Simulation Results 24
3.1.2 Partial Carrier Filling (PCF) Technique for SPM mitigation 26
3.1.2.1 Concept of the Partial Carrier Filling (PCF) Technique 26
3.1.2.2 Simulation Setup 26
3.1.2.3 Simulation Results 28
3.1.3 Subcarrier-Index Modulation (SIM) in CO-OFDM systems . 29
3.1.3.1 Concept of Subcarrier-Index Modulation OFDM (SIM-OFDM) 29
3.1.3.2 Simulation Setup at 10 GS/s with a 256-point IFFT/FFT 31
3.1.3.3 Simulation Results 31
3.1.3.4 Simulation setup at 25GS/s with a 1024-point IFFT/FFT 32
3.1.3.5 Simulation Results 33
3.2 Study of LPN Impact on CO-OFDM systems with 16-QAM and 1024-point IFFT/FFT 35
3.2.1 Concept of the Self-cancellation Technique 36
3.2.2 Simulation Setup at 1024-point IFFT/FFT with 16-QAM . 37
3.2.3 Simulation Results 37

4 Implementation of CO-OFDM Systems **39**
4.1 Transmission setup of the CO-OFDM system 40
4.1.1 Transmitter setup 40
4.1.2 Transmission Link 41
4.1.3 Receiver setup 41
4.2 Study of DFT-spread CO-OFDM systems 43
4.2.1 Concept of DFT-Spread OFDM 43
4.2.2 Concept of Non-iterative Interpolation Based LPN Mitigation 44
4.2.3 Optical back-to-back Experiments on DFT-spread OFDM Systems 46
4.2.3.1 Experimental Results 46
4.2.4 Subband Spectral Shaping in DFT-spread CO-OFDM Systems 48
4.2.4.1 Modified Spectral-Shaping DFT-spread OFDM (MS-OFDM) 49
4.2.4.2 Experimental Results 50
4.3 Study of the Impact of LPN on CO-OFDM systems with a DFB Laser 52
4.3.1 Two-Stage LPN Mitigation Method 52
4.3.2 Homodyne Experiment with DFB Laser and ECL 54
4.3.3 Self-Homodyne Experiment with A DFB Laser 56

5 Summary **58**

A Experimental Components **60**
A.1 Xilinx Virtex-4 FPGAs 60
A.2 MICRAM DACs 61
A.3 Avanex SD50-DP IQ-MZM 62
A.4 ECL and DFB lasers 63
A.5 Polarization Controllers and 90° Optical Hyprid 64
A.6 Photodiods and Oscilloscope 64
A.7 High Speed Receiver 65
A.8 Fiber Spans 66

Bibliography **67**

List of Figures

1.1 Research interest in optical OFDM in recent years 2

2.1 (a) MCM spectrum diagram, (b) OFDM spectrum diagram 10
2.2 The cyclic prefix method 11
2.3 Correlation function results: blue line for real data, red line for imaginary data 13
2.4 Received OFDM signal with a CFO 14
2.5 One OFDM frame structure 17
2.6 : Illustration of the PAPR 20

3.1 Optical OFDM spectrum with an RF-Pilot 23
3.2 System setup of a homodyne CO-OFDM transmission 23
3.3 OFDM demodulation process with the RFP method 24
3.4 BER as function of PSR with different OSNR (a) 128-point FFT/IFFT (b) 256-point FFT/IFFT (c) 512-point FFT/IFFT and (d) 1024-point FFT/IFFT 25
3.5 Four schemes of subcarrier filling for PCF 27
3.6 Four schemes of subcarrier filling for PCF 28
3.7 Subcarrier-index modulation OFDM with 16-QAM and a 1024-point IFFT/FFT 30
3.8 The OFDM demodulation process with the RFP method and SIM demodulation 31
3.9 (a) System Q-factor vs. optical launch power over an 800 km length of fiber, (b) System Q-factor vs. fiber length at a 0 dBm launch power 32
3.10 System setup: (PCF or SC) is not applied with No Comp. In the nonlinearity effect scheme, biasing MZM to add RFP is also not applied, (PBC, PBS, X spans) blocks are not applied with the evaluation of LPN. The coherent detection block consists of a 90° hybrid and two balance photodetectors; The RFP Comp. block is applied only with the evaluation of LPN 33
3.11 (a) System Q-factor vs. optical launch power over an 800 km fiber length, (b) System Q-factor vs. the fiber length at launch power of 0 dBm 34
3.12 Scheme of self-cancellation technique 36
3.13 (a) BER performance for 1 MHz laser linewidth, (b) Required OSNR vs. laser linewidth for $BER = 10^{-3}$ 38

4.1 Experimental setup of the homodyne CO-OFDM system 40
4.2 Experimental setup of the self-homodyne CO-OFDM system 42
4.3 Schematic of a DFT-spread OFDM (a) at the transmitter, (b) in the receiver. The red boxes are removed for conventional OFDM. Legend: S/P=serial to parallel, ZP=zero padding, P/S=parallel to serial, Rem.=remove, PN Comp.=phase noise compensation, either by the CPE or non-iterative interpolation-based method 44
4.4 Example of the non-iterative interpolation-based method with linear interpolation over multiple CPE estimations 45
4.5 Block diagram of the non-iterative interpolation based method . . . 46
4.6 BER vs. RX input power of an N-IFFT/FFT with 1024 points . . . 47
4.7 BER vs. RX input power of the 2048-point N-IFFT/FFT 48
4.8 Spectral-shaping DFT-spread OFDM diagram (S-OFDM) 49
4.9 Modified spectral-shaping DFT-spread OFDM diagram 50
4.10 BER vs. RX input power for DFT-spread OFDM (S-OFDM and MS-OFDM) transmitted over approximately 347 km of fiber 51
4.11 Block diagram of the Two-Stage LPN mitigation method 52
4.12 Received OFDM spectrum for a 1024-point IFFT/FFT at preamplifier input power of 25dBm 53
4.13 System BER vs. optical power at the preamplifier input when the DFB laser is set as the local oscillator 54
4.14 System BER vs. optical power at the preamplifier input when the DFB laser is set at the transmitter 55
4.15 BER vs. optical power at the preamplifier input for the self-homodyne CO-OFDM system 56

A.1 (a) Two Xilinx Virtex-4 FPGAs with a particular power supply, (b) three frequency dividers with a splitter 60
A.2 (a) Two MICRAM DACs with the VEGA evaluation board, (b) the Rohde Schwarz SMP-04 function generator 62
A.3 Avanex SD50-DP IQ-MZM with amplifiers and DC voltage settings 63
A.4 (a) ECL tunable laser, (b) two DFB lasers 63
A.5 (a) Polarization Controller (b) Celight 90° Optical Hybrid 64
A.6 (a) Two differential photodiode pairs with resistive loads, (b) the Tektronix TDS6804B oscilloscope 65
A.7 Polarization-Diversified Optical Hybrid and Two Balanced Photodetectors 66

Abbreviations

ADC	**A**nalog-to-**D**igital **C**onverter
ASE	**A**mplified **S**pontaneous **E**mission
ASIC	**A**pplication-**S**pecific **I**ntegrated **C**ircuit
BER	**B**it-**E**rror-**R**ate
BPF	**B**and-**P**ass **F**ilter
BPSK	**B**inary **P**hase-**S**hift **K**eying
CD	**C**hromatic **D**ispersion
CE	**C**hannel **E**stimation
CFO	**C**arrier **F**requency **O**ffset
CO-OFDM	**C**oherent **O**ptical **OFDM**
CP	**C**yclic **C**refix
CPE	**C**ommon **P**hase **E**stimation
DAC	**D**igital-to-**A**nalog **C**onverter
DCF	**D**ispersion **C**ompensation **F**iber
DDO-OFDM	**D**irect-**D**etection **O**ptical **OFDM**
DFB	**D**istributed **F**eedback **L**aser
DFT	**D**iscrete **F**ourier **T**ransform
DGD	**D**ifferential **G**roup **D**elay
DM	**D**ispersion **M**anaged
DQPSK	**D**ifferential **Q**uadrature **P**hase-**S**hift **K**eying
DSP	**D**igital **S**ignal **P**rocessing
ECL	**E**xternal **C**avity **L**aser
EDFA	**E**rbium **D**oped **F**iber **A**mplifier
FF	**F**ill **F**actor

FFT	**f**ast **F**ourier **T**ransform
FPGA	**F**ield-**P**rogrammable **G**ate **A**rrays
ICI	**I**nter **C**arrier **I**nterface
ICI	**I**nter**C**arrier **I**nterference
IDFT	**I**inverse **D**iscrete **F**ourier **T**ransform
IFFT	**I**nverse **f**ast **F**ourier **T**ransform
IQ-MZM	**IQ** **M**ach-**Z**ehnder **M**odulator
ISI	**I**nter **S**ymbol **I**nterference
ITU	**I**nternational **T**elecommunication **U**nion
LEAF	**L**arge **E**ffective **A**rea **F**iber
LPF	**L**ow-**P**ass **F**ilter
LPN	**L**aser **P**hase**N**oise
LUT	**L**ook**U**p **T**able
MCM	**M**ulti **C**arrier **M**odulation
MGTs	**M**ulti-**G**igabit **T**ransceivers
MS-OFDM	**M**odified **S**pectral shaping DFT-spread **OFDM**
NDM	**N**on-**D**ispersion **M**anaged
NZDSF	**N**on**Z**ero **D**ispersion-**S**hifted **F**iber
OFDM	**O**rthogonal **F**requency-**D**ivision **M**ultiplexing
OOK	**O**n-**O**ff **K**eying
OSNR	**O**ptical-to-**S**ignal **R**atio
PAPR	**P**eak-to-**A**verage-**P**ower **R**atio
PC	**P**olarization **C**ontroller
PCF	**P**artial **C**arrier **F**illing
PDM	**P**olarization-**D**ivision **M**ultiplexing
PMD	**P**olarization-**M**ode **D**ispersion
PPM	**P**ulse **P**osition **M**odulation
PRBS	**P**seudo-**R**andom **B**inary **S**equence
PSR	**P**ilot-to-**S**ignal **R**atio
PTS	**P**artial **T**ransmit **S**equence
QAM	**Q**uadrature **A**mplitude **M**odulation

Q-factor	**Q**uality **factor**
QPSK	**Q**uadrature **P**hase-**S**hift **K**eying
RFP	**R**adio **F**requency **P**ilot
SC	**S**elf **C**ancellation
SE	**S**pectral **E**fficiency
SIM-OFDM	**S**ubcarrier-**I**ndex **M**odulation **OFDM**
SLM	**S**elective **M**apping
S-OFDM	**S**pectral shaping of DFT-spread **OFDM**
SPM	**S**elf-**P**hase **M**odulation
SSMF	**S**tandard **S**ingle-**M**ode **F**iber
VOA	**V**ariable **O**ptical **A**ttenuator
WDM	**W**avelength-**D**ivision **M**ultiplexing
XPM	**C**ross **P**hase**M**odulation

Symbols

ΔCP	Cyclic prefix duration (s)
Δf	the subcarrier spacing (Hz)
ϵ	estimated carrier frequency offset (rad)
γ	nonlinear coefficient ($W^{-1}\ km^{-1}$)
$\Im$	fast Fourier transform
$\hat{\phi_k}$	phase shift due to CD on subcarrier k (rad)
ϕ_0^i	Phase shift due to CPE (rad)
ϕ_{cpe}	Estimated phase shift due to CPE (rad)
φ	phase noise due to ICI (rad)
π	Pi (=3.14159265359)
τ_{ch}	dispersion of channel impulse response
c	Speed of Light (= 299 792 458m/s)
CPE_i	Common Phase Error in the ith OFDM symbol
D_c	Cumulative chromatic dispersion (ps/nm)
f	Frequency (Hz)
f_c	Optical carrier frequency (Hz)
f_k	Frequency of subcarrier k (Hz)
f_{LD}	Transmitter laser frequency (Hz)
F_s	sampling rate/frequency (Hz)
H_k	Transfer function of the fiber at kth subcarrier
k	Subcarrier index
M	Modulation states
n_k	Added Gaussian noise of kth subcarrier

N_{act}	Number of active subcarriers
N_{cp}	Number of CP samples
N_p	Number of pilots
N_{sc}	Number of subcarriers (Number of samples inside the FFT interval)
N_{sym}	Number of OFDM symbol in one OFDM frame
N_{tr}	Number of Training Symbols in one OFDM frame
N_{uti}	Number of utilized subcarriers
N_z	Number of zeros needed due to oversampling
P_{ofdm}	Average power of the OFDM signal (dBm)
P_{rfp}	RF-pilot power (dBm)
Ps_L	L-number of spectral components of phase noise estimation
PN_k^i	Phase noise due to ICI
R_{1k}	Received kth subcarrier 1st training symbol
R_{2k}	Received kth subcarrier 2nd training symbol
R_b	Bit rate (b/s)
R_s	Symbol/Baud rate (baud)
$s(t)$	Transmitted OFDM signal
S_{ofdm}	Spectral efficiency of OFDM (bits/s/Hz)
S_{ook}	Spectral efficiency of OOK (bits/s/Hz)
S_{pcf}	Spectral efficiency of PCF (bits/s/Hz)
S_{sc}	Spectral efficiency of self-cancellation (bits/s/Hz)
$S_{sim-ofdm}$	Spectral efficiency of SIM-OFDM (bits/s/Hz)
t	Time (s)
T_{cp}	CP period (s)
T_s	Symbol duration (s)
T_{sa}	Sampling period (s)
X_k	Transmitted data at frequency of kth subcarrier
$y(t)$	Received data in time domain
Y_k	Received data in frequency domain of kth subcarrier
$\grave{Y}_k^i$	OFDM-received data after channel correction
$\hat{Y}_k^i$	CE and PN compensated OFDM-received data

To my father, ***Hussein Ahmed****, who passed away recently, he would have been very happy to see me, that I received a Ph.D, I miss you dad.*

To my mother, ***Ilham Al-Quraishi****, for her support throughout my life and to my brother* ***Maadh****.*

To my lovely wife, ***Rasha Al-Naseri****, for inspiring me and effortlessly helping me and my beautiful daughters,* ***Dania*** *and* ***Riam****, who make my life full of happiness.*

Chapter 1

Introduction

1.1 Overview

Optical communication is generally divided into single- and multi-carrier communication. The first is a conventional scheme that dominated optical communication in recent decades. The main idea of single-carrier modulation is to use only one carrier to carry the data by modifying one of the signal parameters (e.g., amplitude, frequency, and phase). Multi-carrier modulation employs several carriers to carry the data after dividing them into many low-rate streams, such as in orthogonal frequency-division multiplexing (OFDM) modulation.

The recent research in optical OFDM communication has increased dramatically because of its high spectral efficiency among the technologies that compose the next generation of optical communication systems. The ease of chromatic dispersion (CD) and polarization-mode dispersion (PMD) compensations are major advantages of an optical OFDM system compared to a single-carrier optical system; however, these compensations must be effectively considered in the optical OFDM systems. Optical OFDM systems are mainly divided into coherent optical OFDM (CO-OFDM) and direct-detection optical OFDM (DDO-OFDM) systems.

The growth of interest in optical OFDM in recent years can be observed through the number of hits on the Google Scholar search engine. As shown in Figure 1.1, research on optical OFDM gradually increased from 2006 to 2012. The simulation and experimental studies on CO-OFDM are pursued more actively by researchers compared to DDO-OFDM. This trend can be observed by the number of hits

in Google Scholar (412) for CO-OFDM in 2012 compared to only 108 hits for DDO-OFDM. This higher interest in CO-OFDM is because DDO-OFDM requires a guard band between the optical carrier and OFDM signal, resulting in a low spectral efficiency and making DDO-OFDM less attractive than CO-OFDM.

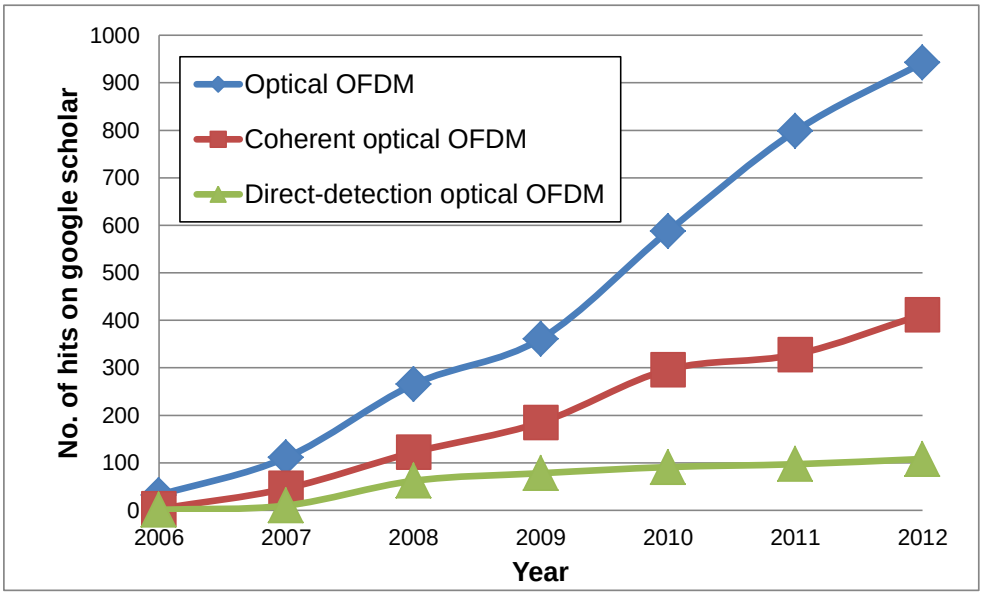

FIGURE 1.1: Research interest in optical OFDM in recent years

1.2 Motivation

CO-OFDM combines two powerful techniques: coherent detection and OFDM. It provides numerous performance advantages, such as (1) high spectral efficiency because OFDM subcarriers are partially overlapped, (2) the possibility of solving the CD and PMD using the cyclic prefix (CP), and (3) low computational complexity of the digital signal processing (DSP) due to the use of an efficient algorithm for inverse discrete Fourier transform (iDFT)/discrete Fourier transform (DFT). The main drawback is a lower tolerance to fiber nonlinearities compared to single-carrier modulation because of the high peak-to-average-power ratio (PAPR). The PAPR drives the optical fiber into a significantly nonlinear region and impacts the limited resolution of digital-to-analog converters (DACs). In particular, longer

OFDM symbols, which are desirable to overcome the overhead required for CP, have a higher PAPR.

In addition, CO-OFDM suffers from laser phase noise (LPN), which strongly degrades the quality of the received signal. This impact becomes more evident with longer OFDM symbols and a lower sampling rate. Moreover, high-order modulation formats, such as 16-quadrature amplitude modulation (QAM), suffer more severely from LPN. The impact of LPN is higher due to the large linewidths of lasers, such as the cost-effective distributed feedback (DFB) laser. Therefore, most current experiments have employed external cavity lasers (ECLs) with a linewidth of approximately 100 kHz at the expense of higher cost. Many recent studies have also considered CO-OFDM systems with 4-QAM and short OFDM symbols, such as a 256-point inverse fast Fourier transform (IFFT)/fast Fourier transform (FFT), to alleviate this impact. Unfortunately, a large portion of the symbol duration of such systems is consumed by CP.

The motivation of this thesis is to investigate the current techniques to combat LPN for such a high-order modulation format with long OFDM symbols and to increase the tolerance of fiber nonlinearities for long-haul CO-OFDM systems. The contributions of the dissertation include performing simulations using VPI-TransmissionMaker with MATLAB and the experimental implementation of a CO-OFDM transmission system.

This thesis is organized into five chapters. A brief description of the OFDM principle is provided in Chapter 2. The principles of OFDM orthogonality, the benefit of the DFT and FFT in OFDM, the principle of the cyclic prefix, and OFDM spectral efficiency are explained. Chapter 2 also addresses the DSP algorithms of CO-OFDM systems, such as window synchronization, carrier frequency offset (CFO), channel estimation and correction, the impact of LPN, and PAPR reduction techniques.

Chapter 3 details the simulation study of the CO-OFDM system using VPITransmissionMaker and MATLAB, where several nonlinearity mitigation techniques are conducted to mitigate self-phase modulation (SPM) and cross-phase modulation (XPM). Furthermore, the LPN impact on the large IFFT/FFT size with a high-order modulation format has been mitigated to enable the usage of a low-cost DFB laser.

Chapter 4 concentrates on the implementation of the CO-OFDM system, starting with the transmission setup of the system. A DFT-spread CO-OFDM system, which has a higher tolerance to fiber nonlinearities, is examined by focusing on the impact of LPN. Two types of CO-OFDM systems with DFB lasers are investigated in Chapter 4 with different LPN mitigation techniques. Finally, Chapter 5 presents the conclusions.

1.3 Publications

The simulation and experimental results that present in this dissertation have been published in reputed photonics journals and conferences. These publications are listed here in addition to my contributions with the other publications.

1.3.1 Journal Papers

- B. Koch, R. Noé, V. Mirvoda, D. Sandel, **O. Jan**, K. Puntsri, "20-Gb/s PDM-RZ-DPSK Transmission with 40 krad/s Endless Optical Polarization Tracking", *IEEE Photonics Technology Letters*, Vol. 25, No. 9, 2013

- **O. Jan**, D. Sandel, K. Puntsri, A. Al-Bermani, M. El-Darawy, and R. Noé, "The robustness of subcarrier-index modulation in 16-QAM CO-OFDM system with 1024-point FFT", *Optics Express*, Vol. 20, Issue 27, pp. 28963-28968, 2012

1.3.2 Conference Papers

- **O. Jan**, K. Puntsri,D. Sandel, A. Al-Bermani, C. Wördehoff, U. Rückert, R. Noé, "An Experiment of Subband Spectral Shaping in DFT-Spread CO-OFDM systems," *10th Conference on Lasers and Electro-Optics Pacific Rim, and The 18th OptoElectronics and Communications Conference / Photonics in Switching 2013 (CLEO-PR&OECC/PS 2013)*, Kyoto, Japan, 2013.

- K. Puntsri, **O. Jan**, A. Al-bermani, D. Sandel,C. Wördehoff, S. Hussin, M. F.Panhwar, U. Rückert and R. Noé, "Pilot-aided CD and PN Compensation Simultaneously in CO-OFDM Systems," *10th Conference on Lasers*

and Electro-Optics Pacific Rim, and The 18th OptoElectronics and Communications Conference / Photonics in Switching 2013 (CLEO-PR&OECC/PS 2013), Kyoto, Japan, 2013.

- B. Koch, R. Noé, V. Mirvoda, D. Sandel, K. Puntsri, **O. Jan** and S. Hussin, "40-krad/s-Fast Polarization Demultiplexing in a 430-km, 20-Gb/s-PDM-RZ-DPSK Transmission," *10th Conference on Lasers and Electro-Optics Pacific Rim, and The 18th OptoElectronics and Communications Conference / Photonics in Switching 2013 (CLEO-PR&OECC/PS 2013)*, Kyoto, Japan, 2013.

- K. Puntsri, **O. Jan**, A. Al-Bermani, C. Wördehoff, D. Sandel, M. Panhwar, S. Hussin, U. Rückert, R. Noé, "ISI Tolerance of Cyclic Prefix Free Coherent Optical OFDM Communication systems," *14. Photonic Networks ITG Symposium*, Proceedings. VDE, 2013.

- **O. Jan**, A. Al-Bermani, K. Puntsri, D. Sandel, C. Wördehoff, U. Rückert, R. Noé, "An Experiment of Coherent Optical DFT-spread OFDM with Laser Phase Noise," *14. Photonic Networks ITG Symposium*, Proceedings. VDE, 2013.

- A. Al-Bermani, C. Wördehoff, **O. Jan**, K. Puntsri, MF. Panhwar, U. Rückert, R. Noé, "The Influence of Laser Phase noise on Carrier Phase Estimation of a Real-Time 16-QAM Transmission with FPGA Based Coherent Receiver," *14. Photonic Networks ITG Symposium*, Proceedings. VDE, 2013.

- B Koch, R Noé, V Mirvoda, D Sandel, **O. Jan**, K Puntsri, "bertragung von 20-Gb/s-PDM-RZ-DPSK mit automatischem optischen Polarisationsdemultiplex bei Polarisationsnderungen bis 40 krad/s," *14. ITG-Fachtagung "Photonische Netze"*, 6.-7. Mai 2013, Leipzig, ITG-Fachbericht.

- **O. Jan**, D. Sandel, M. El-Darawy, K. Puntsri, A. Al-Bermani and R. Noé, "Phase Noise Robustness of SIM-OFDM in CO-OFDM Transmission," *Proc. European Conference on Optical Communication (ECOC2012)*, Amsterdam, The Netherlands, 16.-20. Sept. 2012

- A. Al-Bermani, C. Wördehoff, **O. Jan**, K. Puntsri, U. Rückert and R. Noé, "Real-time Comparison of Blind Phase Search with Different Angle Resolutions for 16-QAM," *IEEE Photonics 2012 Conference (IPC12)*, formerly (LEOS), 23. -27. Sept. 2012, San Francisco, California, USA

- K. Puntsri, V. Mirvoda, S. Hussin, **O. Jan**, A. Al-Bermani, M. F. Panhwar and R. Noé, "A Low Complexity and High Accuracy Frame Synchronization for Optical OFDM and PolMux-Optical OFDM," *IEEE Photonics 2012 Conference (IPC12)*, formerly (LEOS), 23. -27. Sept. 2012, San Francisco, California, USA

- **O. Jan**, D. Sandel, M. El-Darawy, K. Puntsri, A. Al-Bermani, and R. Noé, "Fiber Nonlinearity Tolerance of SIM-OFDM in CO-OFDM Transmission," in *Proc. Conf. 17th Opto-Electronics and Communications Conference OECC 2012*, Paper P1-14, 2. -6. July 2012, Busan, South Korea

- K. Puntsri, D. Sandel, S. Hussin, **O. Jan**, A . Al-Bermani, M. F. Panhwar, and R. Noé, "A Novel Method for IQ Imbalance Compensation in CO-OFDM Systems," in *Proc. Conf. 17th Opto-Electronics and Communications Conference OECC 2012*, Paper 4B3-1, 2. -6. July 2012, Busan, South Korea

- A. Al-Bermani, C. Wördehoff, K. Puntsri, **O. Jan**, U. Rückert, R. Noé, "Phase Estimation Filter Length Tolerance for Real-Time 16-QAM Transmission System Using QPSK Partitioning," *Workshop der ITG-Fachgruppe 5.3.1*, 5-6. July 2012, Gewerkschaftshaus Nrnberg, Germany

- K. Puntsri, V. Mirvoda, S. Hussin, **O. Jan**, A. Al-Bermani, M. F. Panhwar, R. Noé, "A Low Complexity and High Accuracy Frame Synchronization for PolMux-Optical OFDM," *Workshop der ITG-Fachgruppe 5.3.1*, 5. -6. July 2012, Gewerkschaftshaus Nrnberg, Germany

- **O. Jan**, M. El-Darawy, A. Al-Bermani, K. Puntsri, R. Noé, "Mitigation of Fiber Nonlinearities in CO-OFDM Systems," *13. ITG-Fachtagung "Photonische Netze"*, 7.-8. Mai 2012, Leipzig, ITG-Fachbericht 233, P3, pp. 170-172, ISBN 978-3-8007-3437-5

- A. Al-Bermani, C. Wördehoff, K. Puntsri, **O. Jan**, U. Rückert, R. Noé, "Real-time Synchronous 16-QAM Optical Transmission System Using Blind Phase Search and QPSK Partitioning Carrier Recovery Techniques," *13. ITG-Fachtagung "Photonische Netze"*, 7. -8. Mai 2012, Leipzig, ITG-Fachbericht 233, P12, pp. 231-215, ISBN 978-3-8007-3437-5

- **O. Jan**, M. El-Darawy, K. Puntsri, A. Al-Bermani, R. Noé, "RF-pilot-based nonlinearity compensation in frequency domain for CO-OFDM transmission," *Proc. SPIE*, Vol. 8434, Paper 8434-18, 16. -19. April 2012, Brussels, Belgium

Chapter 2

Fundamentals of CO-OFDM

This chapter provides a brief description of OFDM principles and the concepts of associated DSP algorithms. It is organized into two sections. Section 2.1 presents the basic idea of OFDM. First, it clarifies the orthogonality between subcarriers, and then, it explains the DFT process, cyclic prefix, and spectral efficiency of OFDM. Section 2.2 focuses on the DSP algorithms employed by OFDM systems to correct and mitigate the impairments due to the transceiver and channel. It begins by detailing the conventional methods of window synchronization, carrier frequency offset (CFO), and channel estimation. It continues with the LPN impact on which this dissertation is focused and ends with a description of the PAPR.

2.1 Principles of OFDM

OFDM is a digital modulation method that is descended from multi-carrier modulation (MCM), where data are modulated onto many low-rate subcarriers in parallel. These subcarriers are partially overlapped in the frequency domain and are referred to as orthogonal subcarriers. The idea behind MCM is to divide the high-rate data into parallel low-rate data that is modulated over several subcarriers. This parallel scheme leads to a decrease in the effect of intersymbol interference (ISI) in the channel as the symbol rate of the subcarrier is less than the symbol rate of the data [1].

2.1.1 Principle of Orthogonality

As OFDM belongs to the MCM class, the MCM-transmitted signal can be described as [2, 3]

$$s(t) = \sum_{i=-\infty}^{+\infty} \sum_{k=1}^{N_{sc}} x_{ki} c_k (t - iT_s) \tag{2.1}$$

$$c_k(t) = \prod(t) e^{j2\pi f_k t} \tag{2.2}$$

$$\prod(t) = \begin{cases} 1 & \text{if } 0<t \leq T_s \\ 0 & \text{if } t \leq 0, t>T_s \end{cases} \tag{2.3}$$

where x_{ki} is the transmitted data, i is the symbol number of the data information, c_k is the waveform of the subcarrier, k is the subcarrier index, N_{sc} is the number of subcarriers (FFT size), f_k is the frequency of the subcarrier,T_s is the symbol period, and $\prod(t)$ is the function of pulse shaping, which is typically rectangular. Channel spacing must be employed between channels to minimize interference, which, in turn, reduces the spectral efficiency due to occupation of excessive bandwidth. Therefore, OFDM introduces the novel idea of orthogonally overlapping the channels to reduce the utilized bandwidth, referred to as orthogonal subcarriers. The resulting correlation between a subcarrier of frequency f_a and another subcarrier of frequency f_b is [2, 3]

$$\delta_{ab} = e^{j\pi(f_a - f_b)T_s} sinc(j\pi(f_a - f_b)T_s) \tag{2.4}$$

if the condition of $f_a - f_b = m/T_s$ (where m is an integer number) is satisfied, then the two subcarrier signals will be orthogonal to each other. At this point, the utilized bandwidth will be significantly reduced, as shown in Figure 2.1.

To completely recover the data at the receiver if there is no intercarrier interface (ICI), a matched filter can be used.

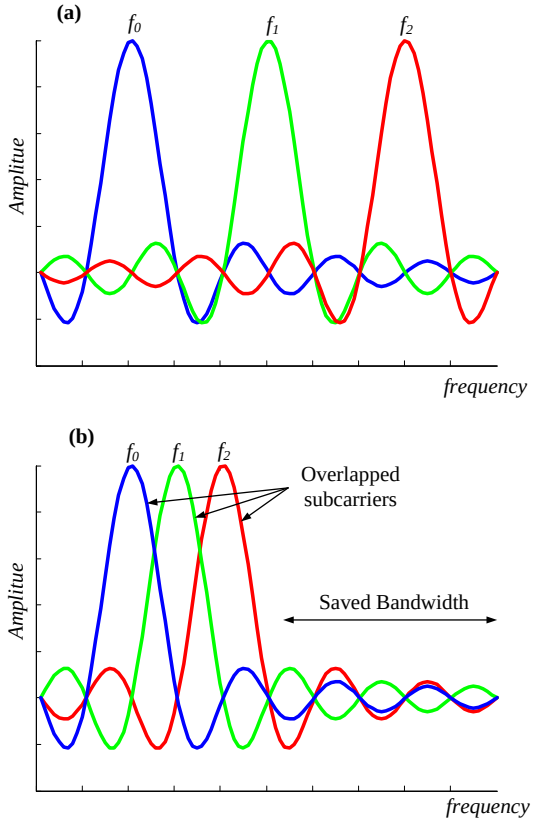

FIGURE 2.1: (a) MCM spectrum diagram, (b) OFDM spectrum diagram

2.1.2 Discrete and Fast Fourier Transform for OFDM

According to Equation 2.1, the transmitter side requires many oscillators to generate the subcarriers and the receiver requires several match filters to recover them. The number of subcarriers must be on the high order to achieve a high tolerance for the fading channel [4]. In practice, this is a significant challenge and leads to a complex architecture. However, OFDM modulation and demodulation can be performed by taking the inverse DFT (iDFT) and DFT of the data, respectively [5]. To reduce the numerical computation time required to take a DFT for long sequences, FFT can be used to yield the same results [6]. Mathematically, using the orthogonality condition, the transmission of one OFDM symbol is [2]

$$s_i = \sum_{k=0}^{N_{sc}-1} X_k e^{j2\pi k(i/N_{sc})} = \Im^{-1}\{x_k\}, \tag{2.5}$$

where $\Im$ is the FFT, and $i \in [0, N_{sc}-1]$. At the transmitter, the DAC converts this discrete signal into a continuous analog signal at the frequency of $1/T_{sa}$, where T_{sa}

is sampling period. While in the receiver, the analog-to-digital converter (ADC) converts the received signal back into discrete values, followed by the inverse of Equation 2.5 to recover the data.

2.1.3 Cyclic Prefix (CP)

In optical communications, the CD and PMD cause a distortion of the transmitted signal that appears as pulse broadening; this phenomenon is referred to as fiber-induced dispersion, which leads to ISI and ICI. Therefore, the CP is a simple solution to eliminate the ISI between consecutive OFDM symbols. The idea behind the CP is to extend the transmitted OFDM signal by ΔCP. This extension can be performed by leading each OFDM symbol with a copy of the last portion of the OFDM signal in the time domain, as shown in Figure 2.2. Therefore, the transmitted signal will be extended by a period of ΔCP, thus reducing the spectral efficiency.

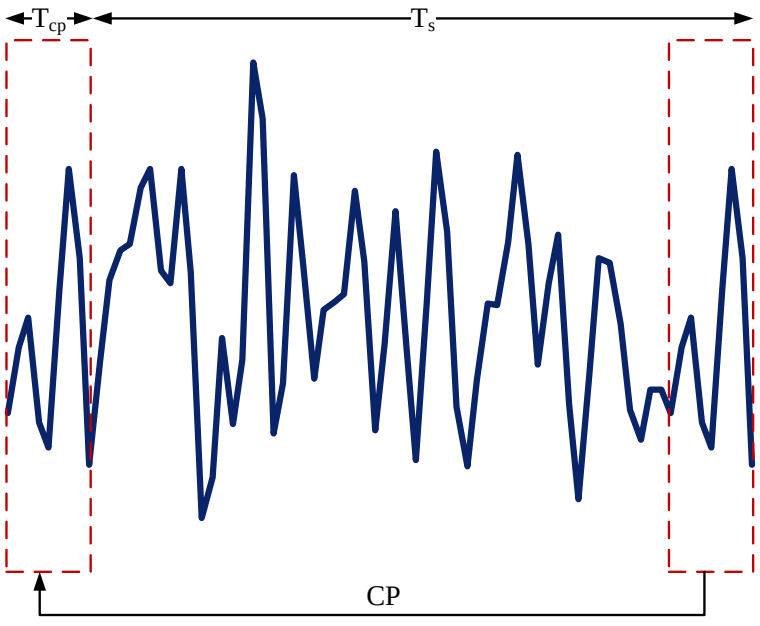

FIGURE 2.2: The cyclic prefix method

The duration of CP (ΔCP) must be longer than the dispersion of the channel impulse response τ_{ch} [2] to completely avoid the ISI of fiber induced dispersion.

$$\Delta CP > \tau_{ch}, \tag{2.6}$$

where τ_{ch} can be given by [7]

$$\tau_{ch} = \frac{c}{f_c^2}|D_c|N_{sc}\Delta f + DGD_{max}, \tag{2.7}$$

where c, f_c, and D_c are the speed of light, the optical carrier frequency, and the accumulated chromatic dispersion, respectively. Δf is the subcarrier spacing, and DGD is the differential group delay of the fiber link. At the receiver, the extension of the CP containing the broadening of the previous OFDM symbol can be easily removed.

2.1.4 Spectral Efficiency (SE)

In general, the symbol rate of the OFDM is given by

$$R_s = \frac{1}{T_s}, \tag{2.8}$$

where T_s is the symbol period including T_{cp} which is the CP period.

Due to the aliasing product induced by the DAC, it is imperative to use zero padding to clearly separate the OFDM signal from the aliasing signal. Excluding Synchronization and training symbols, the maximum achievable spectral efficiency of OFDM, after considering the additional overhead due to the CP and Pilots, can be given by

$$S_{ofdm}[bits/s/Hz] = \frac{N_{sc}}{N_{sc}+N_{cp}} log_2(M) \frac{N_{uti}}{N_{uti}+N_p}, \tag{2.9}$$

where N_{uti} is the number of utilized subcarriers that are used to carry data, N_{cp} is the number of extra samples due to the CP, N_p is the number of pilots and M is the number of modulation states (the symbol alphabet size). N_{sc} is the number of samples inside the FFT interval (number of subcarriers) which is $N_{sc} = N_{uti} + N_p + N_z$, where N_z is the number of zeros needed due to oversampling. The net bit rate of OFDM can be, therefore, written as

$$R_b = F_s S_{ofdm}, \tag{2.10}$$

where F_s is the sampling rate. The spectral efficiency largely depends on the modulation state; the overhead due to the CP and Pilots reduces the spectral efficiency. Hence, several studies have been conducted to reduce or discard the CP [8–12].

2.2 DSP Algorithms for CO-OFDM System

2.2.1 Window Synchronization

Window synchronization is the first step at the receiver after the ADC. In this step, the start position of the FFT window is aligned with the corrected sample. When the start position is not properly detected, the ICI arises between the sub-carriers and induces ISI between the OFDM symbols [2]. The traditional method for window synchronization is the Schmidle-Cox method [13], in which a certain number of OFDM symbols are headed by two identical patterns. Assume one pattern at the transmitter is xp_k, where $k = 1, 2, ..., N_{sc}/2$ therefore the two patterns will be $[xp_k\ xp_k]$.

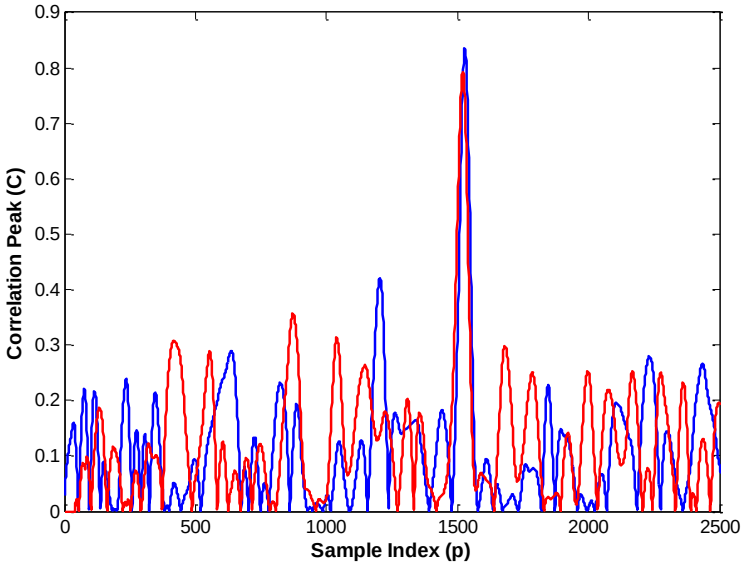

FIGURE 2.3: Correlation function results: blue line for real data, red line for imaginary data

At the receiver, the received data (r) will be correlated by the following function [2, 13]

$$C_p = \sum_{k=1}^{N_{sc}/2} r_{k+p} \cdot r_{k+p+N_{sc}/2} \tag{2.11}$$

The maximum value of the correlation function C_p will determine the start point of the FFT window, i.e., $p = 0$ where p is sample index. Figure 2.3 shows the correlation results of the received two identical symbols of an experimental demonstration of a 1024-point IFFT/FFT at a 5 GS/s sampling rate.

2.2.2 Carrier Frequency Offset (CFO)

The CFO is the impairment induced by the mismatch between a transmitter carrier frequency and local oscillator (LO) frequency in the receiver, as shown in Figure 2.4. This impact results in ICI, which destroys the orthogonality between the subcarriers. In optical communications, because all lasers can produce light over some range of frequencies, the lasers are locked within the International Telecommunication Union (ITU) frequency standard range by wavelength locker, this range has an accuracy of approximately 2.5 GHz. Within this constraint, the frequency offset could be between 5 and 5 GHz [2]. Therefore, frequency offset correction is an imperative step to correct the CFO.

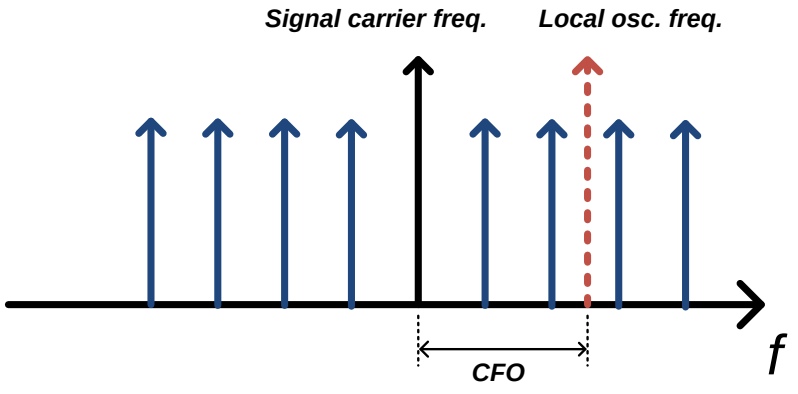

FIGURE 2.4: Received OFDM signal with a CFO

The CFO can be corrected by sending two identical symbols heading the OFDM symbols. To save the overhead, the first OFDM symbol data sends twice in the beginning of the transmission as shown in Figure 2.5; thus, the received pattern after removing the CP is given by [14]

$$r_n = \frac{1}{N_{sc}}[\sum_{k=-K}^{K} X_k \cdot H_k \cdot e^{2\pi jn(k+\epsilon)/N_{sc}}]; n = 0, 1, 2, ..., 2N_{sc}-1, N_{sc} \geq 2K+1 \quad (2.12)$$

where X_k is the transmitted data and H_k is the transfer function of the fiber at the frequency of the kth subcarrier, where K is $N_{sc}/2$. Then the first symbol is

$$R_{1k} = \sum_{n=0}^{N_{sc}-1} r_n \cdot e^{-2\pi jnk/N_{sc}}; k = 0, 1, 2, ..., N_{sc} - 1, \quad (2.13)$$

and the second symbol is

$$R_{2k} = \sum_{n=0}^{N_{sc}-1} r_{n+N_{sc}} \cdot e^{-2\pi jnk/N_{sc}}; k = 0, 1, 2, ..., N_{sc} - 1. \quad (2.14)$$

Therefore, the estimated frequency offset (ϵ) that is a relative frequency offset, which is modulo 1, can be obtained by

$$R_{2k} = R_{1k} \cdot e^{2\pi j\epsilon}. \quad (2.15)$$

self-cancellation is another technique that could be used to CFO correction in mobile communication systems. This technique will be explained later in Section 3.2.1.

2.2.3 Channel Estimation and Correction

The frequency response of a fiber link causes a frequency-dependent phase change due to the chromatic dispersion of the fiber, which is referred to as a CD-induced phase difference between subcarriers [15, 16]. After window synchronization and CFO correction, y_n^i is the received nth sample in the ith OFDM symbol and Y_k^i is the received kth subcarrier after the FFT process in the ith OFDM symbol which are respectively given by [17, 18]

$$\begin{aligned} y_n^i &= x_n^i * h_n^i \cdot e^{j\phi_n^i} + \Im_n^i, \\ Y_k^i &= X_k^i \cdot H_k^i \cdot e^{j\phi_0^i} + \sum_{m=0, m\neq k}^{N_{sc}-1} X_m^i \cdot H_m I_{(m-k)}^i + n_k^i, \end{aligned} \tag{2.16}$$

where x_n^i and X_k^i are the transmitted data and its corresponding frequency domain, $e^{j\phi_0^i}$ and the second term are the impacts of LPN which will be explained in Section 2.2.4, and $\Im_n^i$ and n_k^i are the added Gaussian noise and its corresponding frequency domain. h_n^i and H_k^i are the transfer function of the fiber and its corresponding frequency domain that captures the group velocity delay from the chromatic dispersion, which leads to a phase shift that depends on subcarrier frequency; thus the phase shift can be expressed as [17]

$$H_k^i = |H_k^i| e^{j\hat{\phi_k^i}}, \hat{\phi_k^i} = \pi \cdot c \cdot D_c \cdot (\frac{f_k}{f_{LD}})^2, \tag{2.17}$$

where $\hat{\phi_k^i}$ represents the phase shift due to the CD, D_c is the cumulative chromatic dispersion, and f_k and f_{LD} are the subcarrier and carrier frequencies of the laser, respectively.

This quadratic phase profile can be estimated using a few pilot subcarriers distributed across the OFDM symbol or a few pilot symbols that are termed training symbols heading the OFDM frame. An interpolation between the estimated phase differences of the pilot subcarriers is needed to fill the gaps between the certain pilot subcarriers and to estimate the complete phase profile [19]. Using several training symbols is an attractive method compared to the use of pilot subcarriers because training symbols consider all subcarriers frequencies. Figure 2.5 presents

one OFDM frame with pattern synchronization and training symbols heading the data payload.

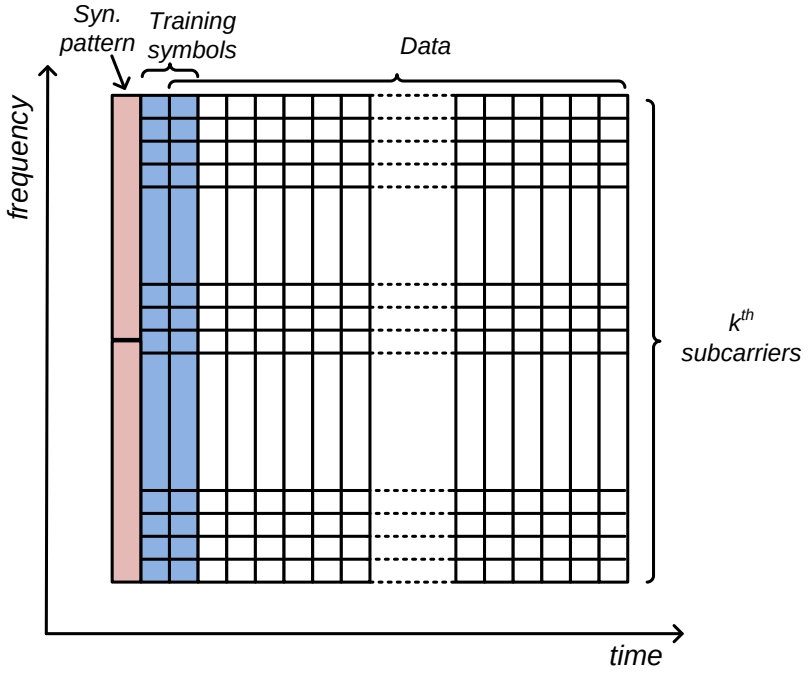

FIGURE 2.5: One OFDM frame structure

In the presence of noise, the accuracy of the estimation can be increased by averaging the estimated frequency difference of each frequency subcarriers across several training symbols which can be expressed as

$$\hat{H}_k = \frac{1}{N_{tr}} \sum_{l=1}^{N_{tr}} \frac{Y_k^l}{X_k^l}, \tag{2.18}$$

where N_{tr} is the number of training symbols considered for one OFDM frame in which the channel transfer function can be expected to be invariant. Therefore large N_{tr} within one OFDM frame would reduce the spectral efficiency at the time of no more improving in the accuracy of the estimation. This indicates two training symbols within one OFDM frame would be sufficient to accurate channel estimation.

2.2.4 Laser Phase Noise (LPN)

LPN is caused by the linewidth of the transmitter and receiver lasers. In CO-OFDM, LPN severely degrades the systems bit error rate (BER) performance due to its longer symbol duration compared to single-carrier modulation. Therefore, LPN is one of the impacts that have been studied in the simulations and experiments presented in Sections 3.2 and 4.3, respectively.

In contrast to the ICI-induced phase difference in Section 2.2.3, LPN varies according to the OFDM symbol. As in Equation 2.16, there are two terms of LPN impact. The first term, ϕ_0^i, is a common phase error (CPE) in ith OFDM symbol, in which the phase rotation is common (that is reflected by 0) for all subcarriers in one OFDM symbol. This phase shift can be estimated using pilot subcarriers, referred to as CPE compensation, if the vector of pilots at the transmitter per OFDM symbol is $XP = [XP_1, XP_2, ..., XP_{N_p}]$ and in the receiver is $YP = [YP_1, YP_2, ..., YP_{N_p}]$, then the phase difference can be calculated as [20]

$$CPE_i = \phi_{cpe}^i = arg(\frac{1}{N_p}\sum_{kp=1}^{N_p}\{YP_{kp}^i \cdot conj(XP_{kp}^i)\}), \tag{2.19}$$

where N_p is the number of pilot subcarriers in ith OFDM symbol, XP, YP are pilot subcarrier amplitudes at the transmitter and in the receiver respectively, and $conj(.)$ is the complex conjugate. This estimated phase shift (ϕ_{cpe}^i) can be compensated for by

$$\hat{X}_k^i = Y_k^i \cdot e^{-j\phi_{cpe}^i}, \tag{2.20}$$

where $k = 1, 2, ..., N_{sc}$ and $i = 1, 2, ..., N_{sym}$. N_{sym} is number of OFDM symbol per one Frame. In fact, this estimation does not compensate for phase noice in practice, therefore RFP method, which is explained in Section 3.1.1, is the practical technique that is considered in the CO-OFDM experiments in this thesis.

The second term, (PN_k), induces ICI in kth subcarrier, where the phase rotation is subcarrier dependent and caused by interference from other subcarriers.

The second term is given by [17, 18]

$$PN_k^i = \sum_{m=0,m\neq k}^{N_{sc}-1} X_m^i \cdot H_m I_{(m-k)}^i, \tag{2.21}$$

$$I_{m-k}^i = \frac{1}{N_{sc}} \sum_{n=-\frac{N_{sc}}{2}}^{\frac{N_{sc}}{2}-1} e^{j2\pi n(m-k)/N_{sc}} e^{j\varphi_n^i}, \tag{2.22}$$

where I_{m-k}^i is the ICI effect coefficient between two subcarriers and φ_n^i is the phase noise due to ICI of nth subcarrier index in ith ODFM symbol that impacts kth subcarrier. According to this equation, the effect of ICI phase noise is expressed as a convolution in the frequency domain. A relatively large laser linewidth, namely, larger than 1 MHz (with low sampling rate), increases the impact of ICI LPN. In contrast, high-order modulation formats, such as 16-QAM, are more prone to LPN impact compared to 4-QAM.

In practice, the only compensation for the common phase noise as in Equation 2.19 is strongly affected by errors. Therefore, it is additionally imperative to compensate for effect of ICI phase noise within an OFDM symbol using a pilot carrier as explained later in Section 3.1.1.

2.2.5 Peak-to-Average Power Ratio (PAPR)

One of the major drawbacks of OFDM is a high PAPR. According to Equation 2.5, an OFDM signal in the time domain is the sum of independently modulated subcarriers due to the independent phase of each subcarrier; therefore, these sinusoid signals will often combine constructively, as shown by the black solid line in Figure 2.6. Briefly, the peak values of some of the transmitted signals could be much larger than the mean values. Assuming that $s(t)$ is the transmitted signal, the PAPR is given by

$$PAPR(dB) = 10log_{10}(\frac{max[s(t)s^*(t)]}{mean[s(t)s^*(t)}), \tag{2.23}$$

where * denotes the conjugate value. The PAPR drives the optical fiber into a significantly nonlinear region due to the high power and the PAPR also impacts the limited resolution of the DAC. Essentially, longer OFDM symbols are more likely to have PAPR.

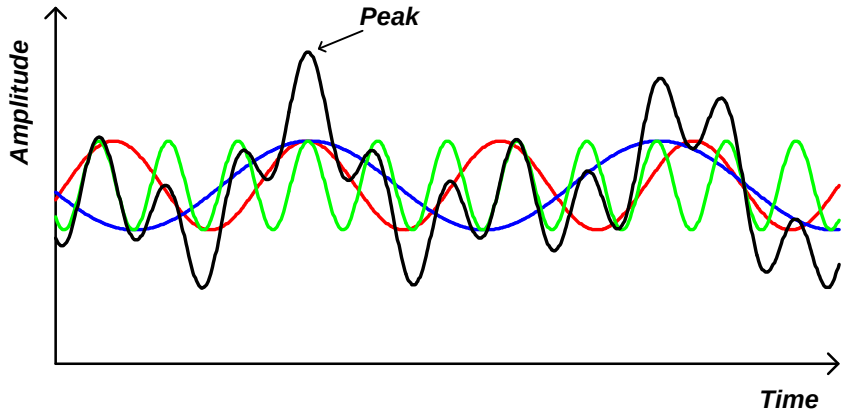

FIGURE 2.6: : Illustration of the PAPR

Several techniques have been proposed in optical OFDM to reduce the PAPR, such as clipping, selective mapping (SLM), and partial transmit sequences (PTS) [21, 22]. These techniques depend on reduction capability and hardware complexity. The first method is the simplest one as it limits the peak envelope of the transmitted signal. However, it leads to signal distortion that is observed as noise. The latter two methods have a high reduction capability at the cost of hardware complexity. Therefore, the results presented in this thesis are based on the clipping method.

Chapter 3

Simulation Study of CO-OFDM Systems

3.1 Study of Fiber Nonlinearities in CO-OFDM Systems

OFDM has a high PAPR compared to the single-carrier modulation format; therefore, the effects of fiber nonlinearities induced by the Kerr effect are a major concern in CO-OFDM systems [23, 24], namely, SPM and XPM. A change in the refractive index of a material such as crystals and glasses due to apply electric field is called Kerr effect. Fiber nonlinearities have a significant effect on such systems because refractive index of the fiber is affected by the intensity of light, and a high electrical peak may increase the variance of the refractive index. To mitigate the effects of fiber nonlinearity, several methods have been proposed to reduce the PAPR of CO-OFDM systems [22, 25]. Nevertheless, the PAPR reduction in a high-speed transmission system becomes unsuitable because the PAPR will quickly increase again due to the accumulated chromatic dispersion [26, 27]. In this section, several methods have been studied for mitigating fiber nonlinearities.

3.1.1 RF-pilot (RFP) method for XPM mitigation

In single-channel transmission, SPM dominates the nonlinear distortion of an OFDM signal, whereas in multi-channel transmission, as in wavelength-division multiplexing (WDM), the XPM between the WDM channels can severely deteriorate the BER performance of the system [28].

Previous studies have demonstrated that the RFP mitigation scheme efficiently compensates for LPN [29, 30]. As the XPM induces a phase distortion in optical system, the RF-pilot scheme can also compensate for fiber nonlinearity [31]. Thus, in this section, the use of the RFP for mitigation of the fiber nonlinearity in CO-OFDM systems is introduced.

3.1.1.1 Concept of the RF-pilot (RFP) method

In the RFP method, a pilot tone is inserted in the middle of the transmitted OFDM signal [29, 31]. The RFP can be easily inserted by turning off the DC subcarrier, whose frequency is equal to optical carrier frequency (i.e when $N_{sc} = 0$), before iFFT stage. After DAC, a DC offset is inserted by driving the V_{bias} at the IQ modulator. This pilot tone is distorted by the effects of fiber nonlinearities in the same fashion as an OFDM signal.

The value of the pilot-to-signal ratio (PSR) has a major influence on the mitigation efficiency of RFP, as depicted in Figure 3.1; the PSR can be defined as

$$PSR(dB) = 10 \cdot log_{10}(\frac{P_{rfp}}{P_{ofdm}}), \tag{3.1}$$

where P_{rfp} is the power of the RFP and P_{ofdm} is the average power of the OFDM subcarriers. In addition to the power required to generate this pilot tone, a guard band is enforced around it to clearly filter the pilot at the receiver.

3.1.1.2 Simulation Setup

Figure 3.2 presents the setup of the homodyne CO-OFDM system that is considered in this simulation [28]. An electrical OFDM baseband signal is generated by MATLAB. A pseudo-random binary sequence (PRBS) bit stream is mapped into

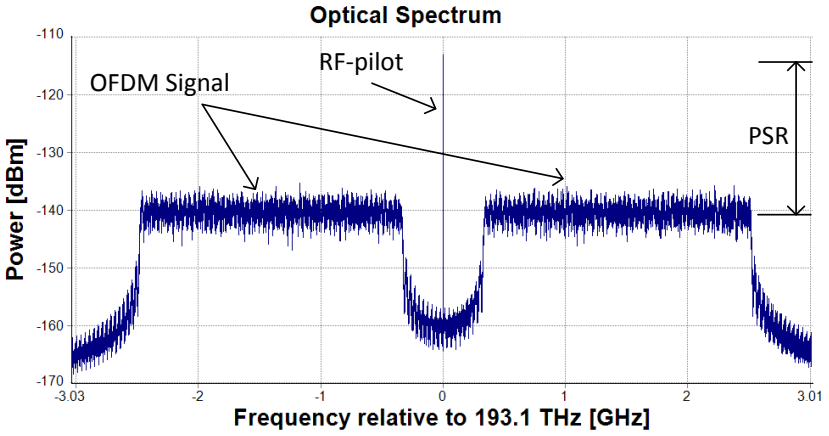

FIGURE 3.1: Optical OFDM spectrum with an RF-Pilot

16-QAM, and then, different sizes of IFFT/FFT with a 12% cyclic prefix for each are used to evaluate the performance of the RFP mitigation. Several training symbols are in the header of the transmission for channel estimation. An optical IQ Mach-Zehnder Modulator (IQ-MZM) converts the electrical signal into an optical signal.

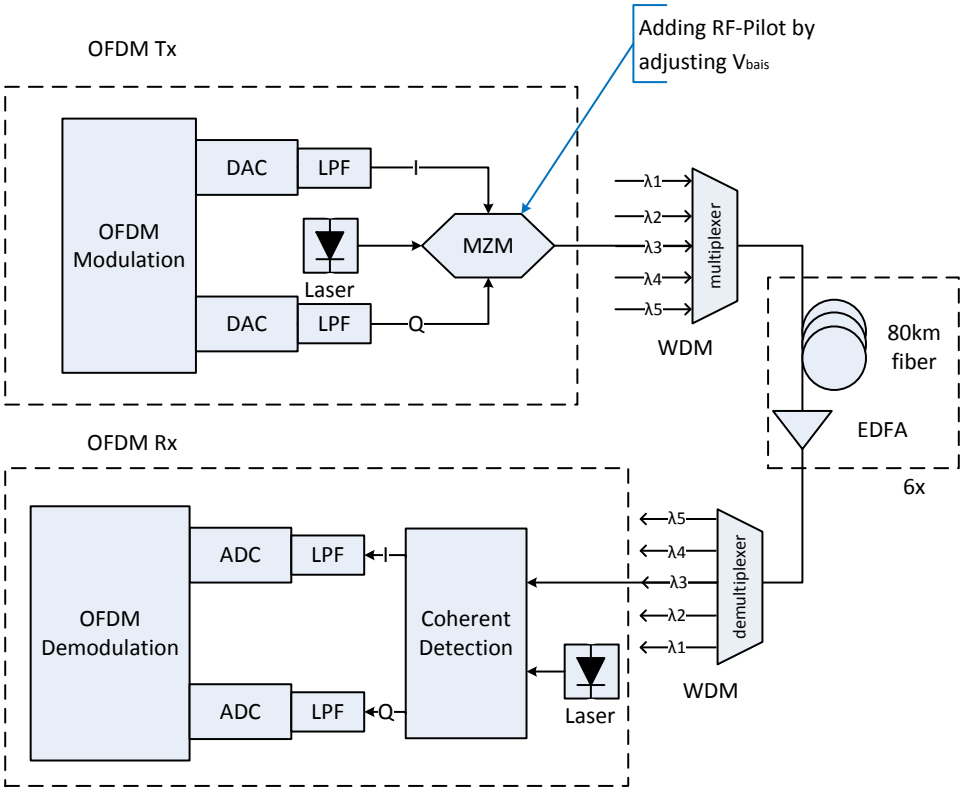

FIGURE 3.2: System setup of a homodyne CO-OFDM transmission

VPITransmissionMaker 8.6 is employed to model the optical transmission at a sampling rate of 5 GS/s. The optical signal is transmitted over six spans; each span consists of 80 km of standard single-mode fiber (SSMF), and an erbium-doped fiber amplifier (EDFA) is required to compensate for the span loss with a gain of 16 dB and a noise figure of 6 dB. The total fiber link is 800 km. The fiber chromatic dispersion of 16 ps/nm/km with a 0.2 dB/km loss and a nonlinear coefficient of $6 \cdot 10^{-20}\ m^2/W$ modeled. Five WDM channels with a channel spacing of 5 GHz are transmitted to evaluate the effect of XPM.

To only evaluate the performance of RFP mitigation against fiber nonlinearities, no phase noise is modeled in the lasers. At the coherent receiver, a 90° optical hybrid mixes the signal with the LO, and then, two balanced photodetectors convert the signal from the optical domain to the electrical domain. Finally, the electrical signal is sent to an OFDM demodulation function, as shown in Figure 3.3, where the RFP for each OFDM symbol is filtered, conjugated, and then multiplied by its OFDM symbol. This procedure is followed by a process to remove the CP and an FFT process to convert the data to the frequency domain. The final steps are channel estimation, channel correction, and BER calculation.

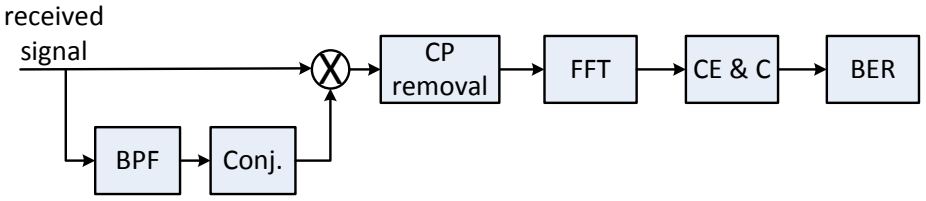

FIGURE 3.3: OFDM demodulation process with the RFP method

3.1.1.3 Simulation Results

It is important to retrieve the best PSR value [28] because the total power of the system is the power of pilot plus the power of the OFDM subcarriers. This results in, when the PSR is excessive, inducing the power of the OFDM subcarriers becomes too low and leads to worse BER performance due to amplified spontaneous emission (ASE) noise. Furthermore, when the RFP power is too low, the ASE noise impacts the BER performance of the RFP compensation; thus, the RFP becomes too noisy to mitigate for the phase distortion. The conventional RFP mitigation [31] requires a guard band around the pilot tone. This guard band

decreases the spectral efficiency. A large guard band could reduce the effect of the mitigation performance because the noise within the guard band around the RFP is multiplied by the OFDM symbols.

Figure 3.4 illustrates the influence of the PSR on the BER. The best PSR is approximately - 6 dB for the 128-, 256-, 512-, and 1024-point IFFT/FFT. This high value indicates that about 1/5 of the power is wasted on the pilot carrier. In addition, as shown in Figure 3.1 about 1/6 of the available bandwidth is lost for the empty channels around the pilot carrier, which in principle the high spectral efficiency of OFDM is remarkably reduced. This reduction can be halved by considering polarization multiplexing and polarization diversity receiver side, because the pilot carrier could be used for both polarizations.

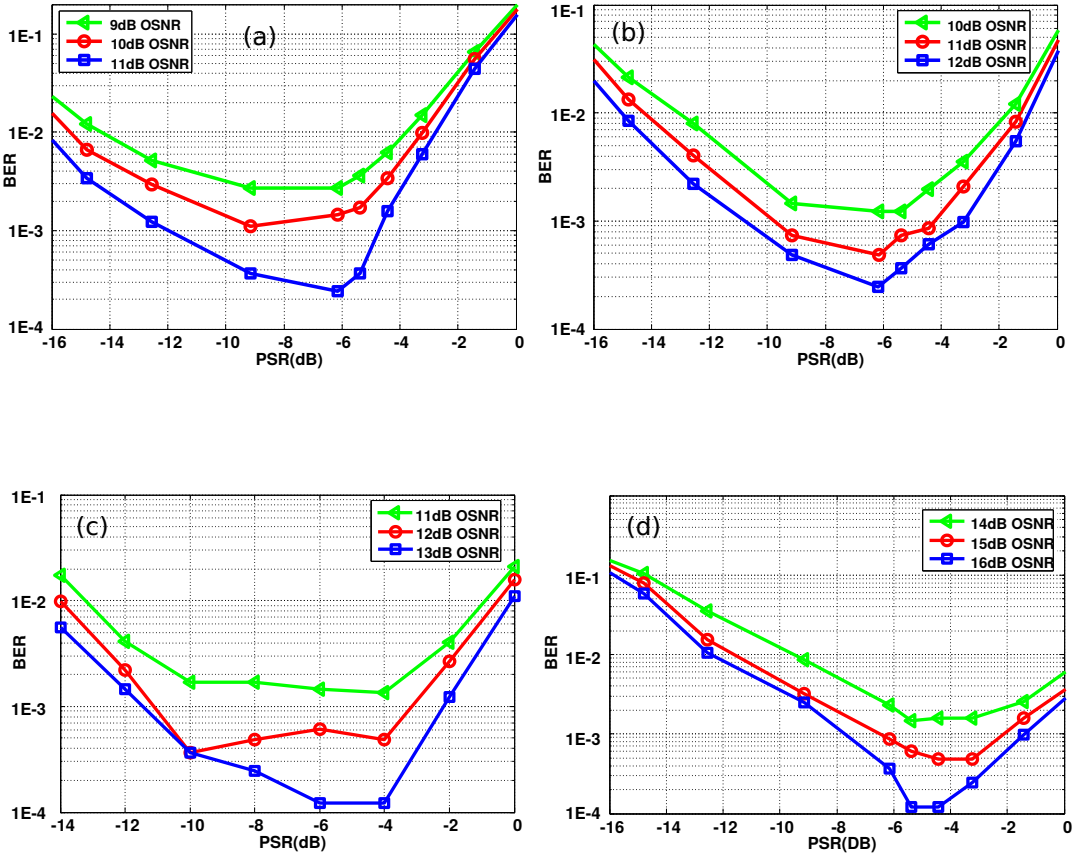

FIGURE 3.4: BER as function of PSR with different OSNR (a) 128-point FFT/IFFT (b) 256-point FFT/IFFT (c) 512-point FFT/IFFT and (d) 1024-point FFT/IFFT

3.1.2 Partial Carrier Filling (PCF) Technique for SPM mitigation

This section verifies that the RFP technique in CO-OFDM systems can efficiently mitigate the fiber nonlinearity induced by XPM but not that induced by SPM. Furthermore, combining the RFP technique with the PCF technique, which can effectively mitigate SPM, is proposed to mitigate fiber nonlinearity in both XPM and SPM [32]. This technique shows better Q-factor (quality factor) than that technique with RFP only as in [31].

3.1.2.1 Concept of the Partial Carrier Filling (PCF) Technique

PCF is an easy technique for mitigating the SPM. The basic idea of PCF is that data are appointed to some adjacent subcarriers followed by off subcarriers (without data). This technique results in part of the distortion because SPM becomes located in the off subcarriers. The fill factor (FF) of PCF is defined as the number of filled subcarriers divided by the total number of subcarriers [33]; a FF of 50% is considered in this thesis. Polarization multiplexing can be employed to minimize spectral efficiency loss. Figure 3.5 presents four schemes of subcarrier filling (50% FF is considered for all schemes) that are investigated to evaluate the BER performance of the system with the PCF technique. According to Equation 2.9, the spectral efficiency of PCF with CP can be expressed as

$$S_{pcf}[bits/s/Hz] = FF \cdot \frac{N_{sc}}{N_{sc}+N_{cp}} \cdot log_2(M)\frac{N_{uti}}{N_{uti}+N_p}, \tag{3.2}$$

where M is the number of modulation states. As observed previously, the spectral efficiency of the PCF technique causes a reduction in bandwidth efficiency by a factor of two if an FF of 50% is used. There are several solutions for reducing this limitation, such as employing PDM or using a large alphabet size. A new modulation format is proposed in Section 3.1.3.

3.1.2.2 Simulation Setup

In this simulation [32], the bit streams are mapped into 16-QAM, 256-points IFFT with 128 zero-padding and a 12% cyclic prefix at 10 GSa/s. These baseband

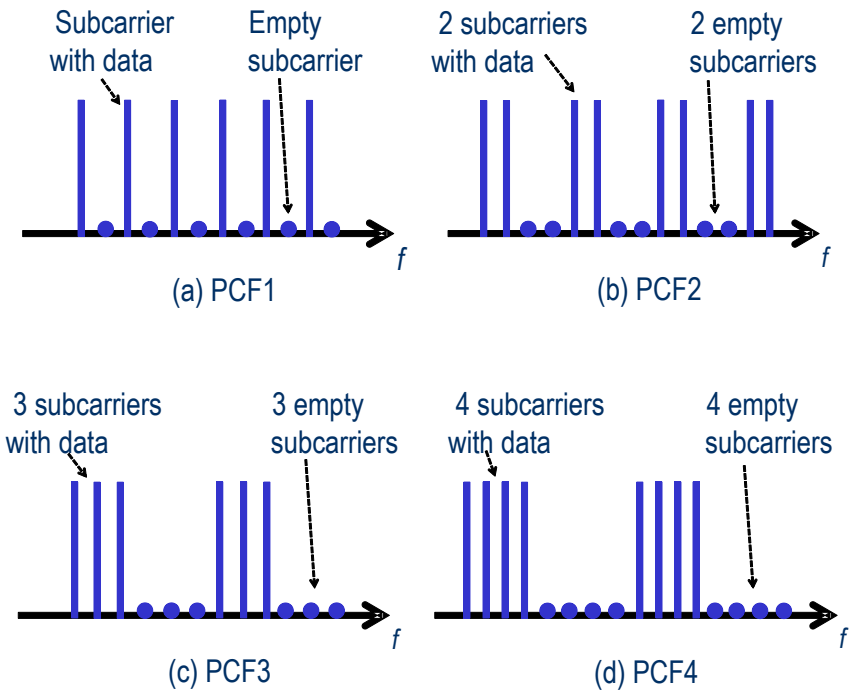

FIGURE 3.5: Four schemes of subcarrier filling for PCF

OFDM signals are fed into an optical IQ-MZM, where a DC offset places the pilot tone in the center of the OFDM spectrum. This simulation compares the RFP only and RFP method combined with various PCF schemes. Thus, the bit rate for the RFP only is 15.52 G bit/s, whereas it is 7.76 G bit/s for the PCF technique because the spectral efficiency is lowered by a factor of two.

The optical transmission link is set by several spans of 80 km SSMF fiber with an EDFA that has a noise figure of 6 dB. A fiber loss of 0.2 dB/km and a nonlinearity parameter (γ) of 1.3 W^{-1} km^{-1} are considered. Five WDM channels with a channel spacing of 50 GHz are employed. To evaluate the tolerance for fiber nonlinearity only, LPN is not modeled.

At the coherent receiver, a 90° optical hybrid mixes the signal with the LO, and then, the optical domain signal is converted into the electrical domain using balanced photodetectors. Finally, the electrical signal is sent to an OFDM demodulation block, where the RFP for each OFDM symbol is filtered, conjugated, and then multiplied by its OFDM symbol. This process is followed by removing the CP, a 265-point FFT block, estimating and correcting the channel, and calculating the BER.

3.1.2.3 Simulation Results

As depicted in Figure 3.6 (a), at a 1 dBm launch power, a quality factor (Q-factor) improvement of approximately 0.5 dB is achieved for schemes PCF3 and PCF4 combined with the RFP compared to schemes PCF2 and PCF1 combined with the RFP. At the same launch power, combining PCF4 with the RFP increases the Q-factor by approximately 2.3 dB compared to the RFP technique alone. This result demonstrates that the RFP technique does not effectively mitigate SPM [32]. This result is consistent with those obtained in [34, 35].

Figure 3.6 (b) presents the system Q-factor vs. fiber length at a 0 dBm launch power. Over 1120 km, where total nonlinearity is considerable, combining PCF4 with RFP yields improvements of approximately 2 and 0.4 dB compared to the RFP technique alone and combining PCF2 with RFP, respectively. It is clear that the combination of PCF4 with RFP appears to have a slightly better Q-factor than the other schemes due to a reduction in both the XPM and SPM penalties.

As a result, the combination of PCF with RFP gives better Q-factor than RFP only because of doubling the adjacent channel spacing which leads to improve mitigation of fiber nonlinearity due to SPM, alongside with mitigating XPM by RFP technique. Q-factor is a measure of signal quality which is directly driven from BER as $BER = 0.5erfc[Q/\sqrt{2}]$, where $erfc[]$ denotes the complementary error function.

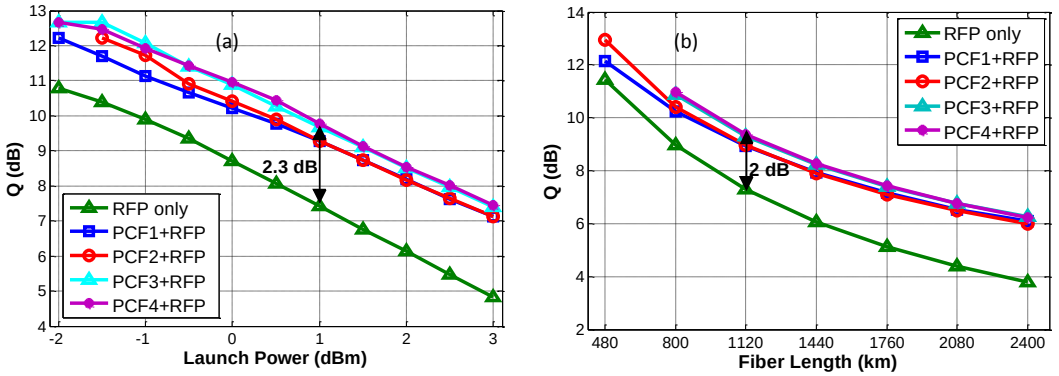

FIGURE 3.6: Four schemes of subcarrier filling for PCF

3.1.3 Subcarrier-Index Modulation (SIM) in CO-OFDM systems

In Section 3.1.2.1, the PCF technique is applied [33] to mitigate the SPM and combined with the RFP to compensate for the XPM. However, PCF degrades the spectral efficiency [36]. Subcarrier-index modulation (SIM) is a new transmission approach that has been integrated with OFDM systems. This approach displays more improvement than the conventional OFDM [37, 38]. In this section, the SIM modulation format for a CO-OFDM system is proposed. The numerical results demonstrate a tolerance to fiber SPM when the RFP is applied to compensate for XPM [36].

3.1.3.1 Concept of Subcarrier-Index Modulation OFDM (SIM-OFDM)

SIM-OFDM employs the subcarrier index in an on-off keying (OOK) scheme to decide whether symbols are transmitted over a subcarrier index [37]. At the transmitter, before the S/P block, the bit stream is split into two subsets. The first subset is for the OOK format, in which the location of each bit is associated with the index state of each subcarrier to activate it (or not). The active subcarriers carry the second subset of the bit stream after mapping by, e.g., 16-QAM while the inactive subcarriers are turned off. This mapping can be performed by adding another block at the transmitter as an SIM-OFDM modulator. Figure 3.7 provides an example of this modulation format in which the bit stream is prepared to the IFFT block, the output of S/P block is provided to IFFT block to convert the signal into time-domain. Thus Figure 3.7 shows frequency-domain before considering IFFT process. After excluding some overhead, the number of bits for the OOK format is equal to the number of subcarriers.

At the receiver, the first step is to retrieve the active and inactive subcarriers to estimate the first subset of bits of the OOK format. The second step is the conventional process of demodulating the OFDM data. The SIM-OFDM technique provides spaces between subcarriers that carry the data.

Assuming 16-QAM and 1024-point IFFT are employed. In OFDM system, N_{sc} subcarriers are transmitted in one OFDM symbol. Let assume the sampling rate is 28 GHz, therefore the frequency space between two subcarriers is $28\ GHz/1024 =$

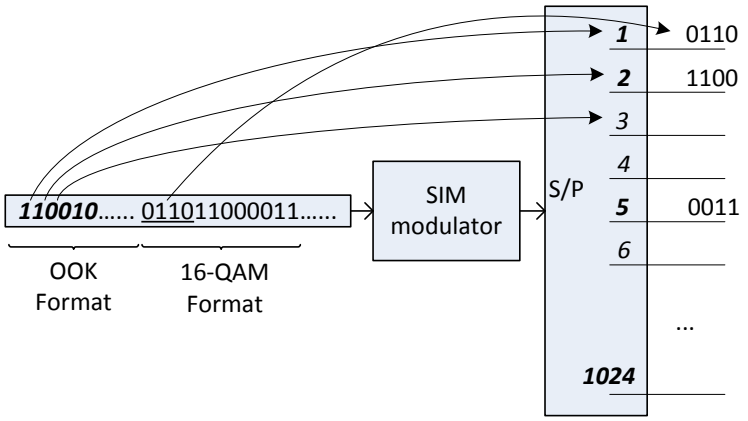

FIGURE 3.7: Subcarrier-index modulation OFDM with 16-QAM and a 1024-point IFFT/FFT

27.3 MHz. The spectral efficiencies of conventional OFDM and SIM-OFDM can be calculated as follows:

Spectral Efficiency of conventional OFDM: 1024 subcarriers are transmitted because of 1024-point IFFT, each subcarrier can convey 4 bits because of 16-QAM mapping, this results in 4096 bits. Therefore the bit rate is 4096 $bits \cdot 27.3\ MHz = 112\ Gbit/s$. Considering that the allocated bandwidth is 50 GHz, then $SP_{ofdm} = 112\ Gbit/s/50\ GHz = 2.24\ bit/s/Hz$.

Spectral Efficiency of SIM-OFDM: Assuming half of N_{FFT} is turned OFF, the active subcarriers are 512. Therefore 2048 bits can be transmitted instead of 4096 bits above. OOK scheme uses 1024 bits to indicate ON, OFF of the subcarrier indexes. The total transmitted bits are 3072 bits. Therefore the bit rate is 3072 $bits \cdot 27.3\ MHz = 83.865\ Gbit/s$. To transmit OOK information, extra bandwidth is needed, it is just as much as for the subcarriers themselves. Therefore $SP_{sim-ofdm} = 83.865\ Gbit/s/(50\ GHz \cdot 2) = 0.84\ bit/s/Hz$.

3.1.3.2 Simulation Setup at 10 GS/s with a 256-point IFFT/FFT

In this simulation, the bit streams are first passed to the SIM-OFDM modulator block. This block determines the active and inactive subcarrier indexes. Then, the data of the second subset are mapped with 16-QAM, a 256-point IFFT/FFT with 128 zero-padding, and a 12% cyclic prefix at a 10 GS/s sampling rate [36].

An IQ-MZM converts the baseband OFDM signals to the optical domain, where a DC offset places the pilot tone in the center of the OFDM spectrum. The optical transmission link is simulated by several spans, each composed of 80 km of SSMF fiber and an EDFA with a noise figure of 6 dB. A fiber loss of 0.2 dB/km and a nonlinear coefficient (γ) of 1.3 W^{-1} km^{-1} are considered. Five WDM channels with a channel spacing of 50 GHz are modeled, as shown in Figure 3.2. To evaluate the tolerance for fiber nonlinearity only, no phase noise from the lasers is modeled.

At the coherent receiver, a 90° optical hybrid is employed to mix the signal with the LO and balanced photo-detectors convert the optical domain back into the electrical domain. Then, the electrical signal is passed to OFDM demodulation, where, for each OFDM symbol, the RFP is filtered by a band-pass filter (BPF), conjugated, and multiplied by its OFDM symbol, followed by removing the CP, performing a 256-point FFT, demodulating the SIM, and calculating the BER, as shown in Figure 3.8.

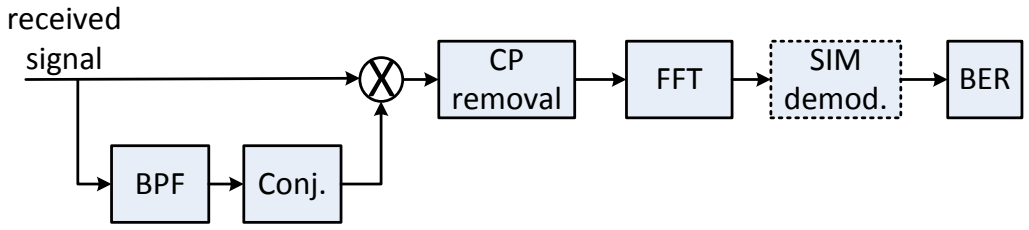

FIGURE 3.8: The OFDM demodulation process with the RFP method and SIM demodulation

3.1.3.3 Simulation Results

Figure 3.9 (a) depicts the Q-factor vs. launch power over an 800 km SSMF fiber [36]. At a launch power of 1 dBm, when total nonlinearity is considerably high,

combining SIM-OFDM with RFP yields a greater-than 1 dB improvement in Q-factor compared to combining PCF with RFP. At the same launch power, combining SIM-OFDM with RFP increases the Q-factor by approximately 2.6 dB compared to the RFP technique alone. As discussed in Section 3.1.2.3, this result demonstrates that the RFP does not effectively compensate for SPM.

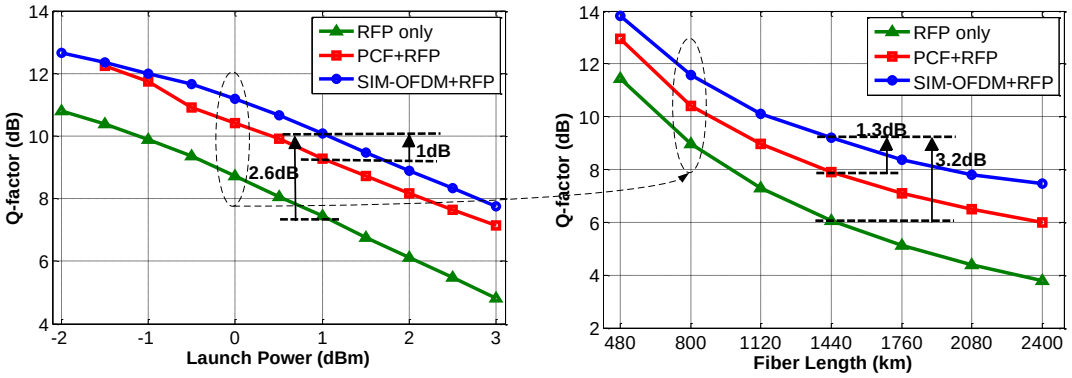

FIGURE 3.9: (a) System Q-factor vs. optical launch power over an 800 km length of fiber, (b) System Q-factor vs. fiber length at a 0 dBm launch power

Figure 3.9 (b) shows the system Q-factor vs. the fiber length at a 0 dBm launch power [36]. After a 1440 km transmission, combining SIM-OFDM with RFP shows a $\sim$ 3.2 dB and $\sim$ 1.3 dB improvement compared to the RFP technique and the combined PCF with RFP, respectively. This result indicates that combining SIM-OFDM with RFP is better than combining PCF with RFP due to reducing both XPM and SPM penalties.

3.1.3.4 Simulation setup at 25GS/s with a 1024-point IFFT/FFT

Figure 3.10 depicts the simulation setup based on VPI TransmissionMaker [39]. The bit streams are mapped to 16-QAM. A 1024-point IFFT/FFT with 512 padded zeros is considered. 20 subcarriers is used for a guard band around the RFP. The cyclic prefix takes 64 samples. The sampling rate is 25 GS/s. This baseband OFDM signal is passed to an optical IQ-MZM that has an extinction ratio of 30 dB, where a DC offset places the pilot tone in the center of the OFDM spectrum. The SE reduction is less than that of PCF and can be cope with by using polarization multiplexing, and/or high order constellation.

The optical transmission link is modeled by several spans, each with 80 km of SSMF fiber with an EDFA that has a noise figure of 6 dB. This simulation

considers a 0.2 dB/km fiber loss, 17 $ps\ nm^{-1}\ km^{-1}$ chromatic dispersion, 0.1 $ps\ km^{-1/2}$ polarization mode dispersion, and a 1.3 $W^{-1}\ km^{-1}$ nonlinear coefficient (γ). Polarization-division multiplexing (PDM) is employed. No Comp. indicates that neither PCF nor SIM-OFDM is applied and that the RFP technique is not employed in this simulation. To only evaluate the tolerance for fiber nonlinearities, the lasers have no phase noise.

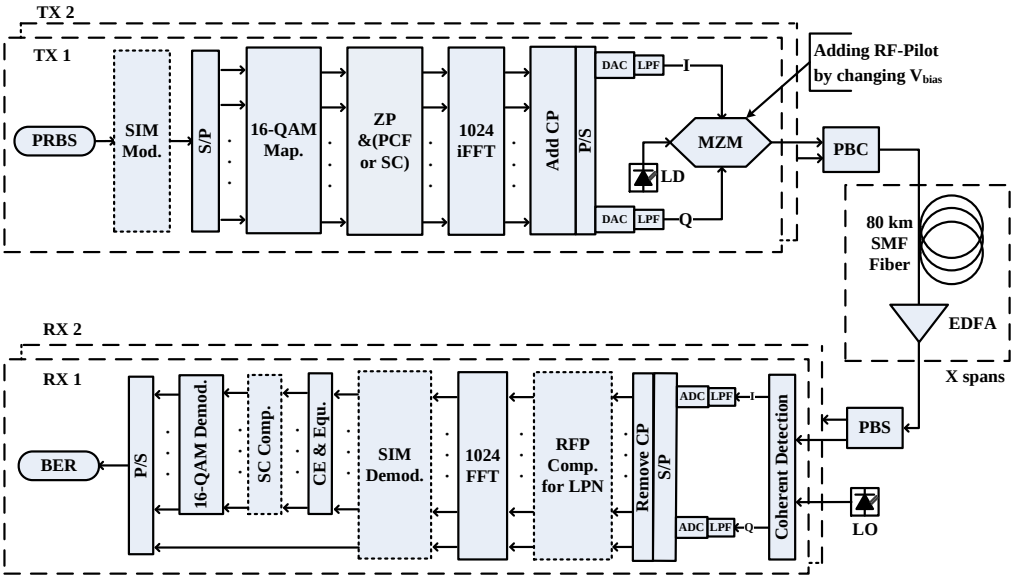

FIGURE 3.10: System setup: (PCF or SC) is not applied with No Comp. In the nonlinearity effect scheme, biasing MZM to add RFP is also not applied, (PBC, PBS, X spans) blocks are not applied with the evaluation of LPN. The coherent detection block consists of a 90° hybrid and two balance photodetectors; The RFP Comp. block is applied only with the evaluation of LPN

3.1.3.5 Simulation Results

Figure 3.11 presents the Q-factor vs. launch power over an 800 km SMF fiber. As total nonlinearity is high, i.e., the launch power is 0 dBm, SIM-OFDM exhibits an approximately 0.5 and 1.5 dB improvement in the Q-factor compared to the No Comp. [39] and PCF technique only, respectively. This result indicates that the SIM-OFDM successfully mitigates the effect of SPM. Figure 3.11 (b) presents the system Q-factor vs. fiber length at a launch power of 0 dBm. Over 1440 km, SIM-OFDM depicts an approximately 1.5 dB improvement compared to No Comp. and a slight improved compared to the PCF technique. These results indicate that SIM-OFDM clearly reduces the penalty due to SPM and can support a long fiber link [39].

As both the SIM-OFDM and PCF techniques accommodate wide separation between the subcarriers, the SIM-OFDM is efficient for high-order constellations with a large IFFT/FFT size and long fiber link compared to the PCF technique [39]. A larger IFFT/FFT size is used to reduce the overhead of the cyclic prefix, which is required to avoid the ISI. After this work, [40] reported a good comparison for the SIM-OFDM format combined with pulse position modulation (PPM); this scheme maintains zeros between subcarriers and has a fixed spectral efficiency. The simulation results provided by [40] are similar to the results of this dissertation.

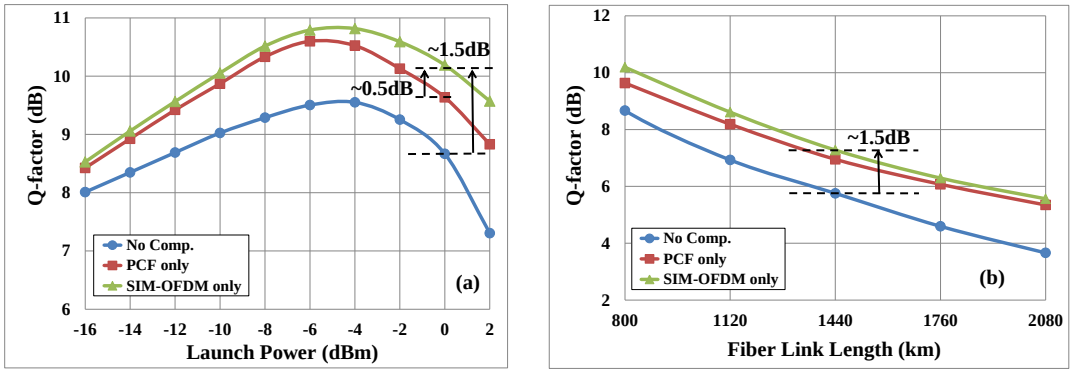

FIGURE 3.11: (a) System Q-factor vs. optical launch power over an 800 km fiber length, (b) System Q-factor vs. the fiber length at launch power of 0 dBm

3.2 Study of LPN Impact on CO-OFDM systems with 16-QAM and 1024-point IFFT/FFT

CO-OFDM suffers from LPN that highly degrades system BER performance. A 93.8 Gb/s transmission with 4-QAM, 1024-point IFFT/FFT, 25 GS/s, and polarization-division multiplexing has recently been realized [41]. A 101.5 Gb/s transmission with 16-QAM, 64-point FFT, 28 GS/s and a single polarization has also been experimentally demonstrated [42]. Furthermore, an experiment with 4-QAM, various IFFT/FFT points from 512 to 4096, 25 GS/s and a single polarization has been studied to investigate the limitation of using large IFFT/FFT points in the presence of LPN [43]. All experiments listed so far have employed ECL with linewidth of $\sim$ 100 kHz. Moreover, when the same sampling rate is employed, compared to 4-QAM, high-order modulation formats such as 16-QAM suffer more severely from LPN. To my knowledge, none of the current experiments has employed DFB lasers that has large linewidths with high-order constellation and large IFFT/FFT points [39, 44].

To use DFB laser, several techniques have been conducted. One elegant technique is the RFP which not only compensate for the impact of LPN but is also able to mitigate fiber nonlinearities as it has been studied in section 3.1.1 [29, 31, 39, 44]. This technique is also employed in most experiments with ECL lasers. In this section, first a limitation of the RFP compensation for large linewidths of lasers with a 16-QAM, 1024-point IFFT/FFT, 25 GS/s system is conducted.

In mobile communication systems, ICI self-cancellation technique shows a good candidate for CFO correction. This CFO is due to the differences between transmitted and received carrier frequencies [45]. These differences induce a loss of orthogonality between subcarriers and leads to ICI. Therefore, second ICI self-cancellation technique is combined with the RFP for LPN compensation to enable the usage of DFB lasers in the CO-OFDM systems. Although ICI self-cancellation significantly reduces the impact of LPN, the significantly lower bandwidth efficiency of this technique is a major disadvantage. Final the SIM-OFDM that is explained in section 3.1.3.1 is proposed to combat LPN. The simulation results depict a tolerance towards LPN, when the SIM-OFDM is combined with the RFP compared to conventional CO-OFDM with the RFP technique.

3.2.1 Concept of the Self-cancellation Technique

As shown in Figure 3.12, the basic idea is to transmit an inverted M-QAM data on pairs of adjacent subcarriers using $X^i(k+1) = -X^i(k)$, where k is the index of the even-numbered subcarrier, i is the OFDM symbol and x is the M-QAM data symbol [39, 44].

$$Y^i_{sc}(k) = Y^i(k) - Y^i(k+1), k \text{ is even.} \tag{3.3}$$

In Equation 3.3, $Y^i_{sc}(k)$ is the data at the receiver after canceling ICI in the frequency domain. This cancellation can be done by subtracting each received odd-numbered data subcarrier $Y^i(k+1)$ from the previous data subcarrier $Y^i(k)$ in the ith OFDM symbol [45].

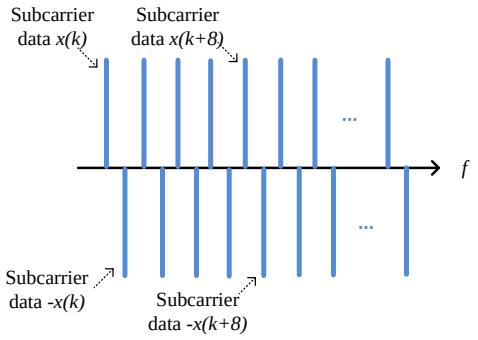

FIGURE 3.12: Scheme of self-cancellation technique

Hence, the residual ICI contained in the received data after the RFP compensation is mitigated because the ICI impacts in channels k and $k+1$ are strongly correlated. For simplicity no extra overhead is assumed (such as CP, training symbols, and pilots), therefore the spectral efficiency of CO-OFDM with self-cancellation technique can be defined as

$$S_{sc}[bits/s/Hz] = \frac{1}{2} \cdot log_2(M), \tag{3.4}$$

where M is the number of modulation states.The self-cancellation technique therefore has only half the spectral efficiency of conventional CO-OFDM system. To overcome this disadvantage, the bandwidth of OFDM signal can be increased or a large alphabet size must be employed.

3.2.2 Simulation Setup at 1024-point IFFT/FFT with 16-QAM

Figure 3.10 depicts the simulation setup based on VPITransmissionMaker. The bit streams are mapped into 16-QAM. A 1024-point IFFT/FFT with 512 padded zeros is employed. 20 subcarriers set as a guard band around the RFP. The cyclic prefix takes 64 samples. The electrical signal is sampled at 25 GS/s. This baseband OFDM signal is sent to an optical IQ-MZM with 30 dB extinction ratio, where a DC offset places the pilot tone in the center of the OFDM spectrum [39, 44]. An optical back-to-back transmission simulation is carried out to evaluate only the laser phase noise impact. Four schemes have been proposed: conventional CO-OFDM combine with the RFP referred to (RFP only), SIM-OFDM combine with the RFP referred to (SIM + RFP), PCF combine with the RFP referred to (PCF + RFP) and the self-cancellation technique with the RFP referred to (SC + RFP). A window synchronization and frequency offset compensation are perfectly assumed in this simulation [39, 44].

3.2.3 Simulation Results

The RFP only is not very effective for high-order modulation format with large IFFT/FFT points and large linewidths of lasers as shown in Figure 3.13 (a), where it barely reaches BER of $1 \cdot 10^{-3}$ at $\sim$ 21.4 dB OSNR when 1 MHz laser linewidth is modeled. Self-cancellation combine with the RFP technique , PCF combine with the RFP technique and SIM-OFDM combine with the RFP technique can easily show $1 \cdot 10^{-3}$ BER at $\sim$ 10.6 dB, $\sim$ 12.6 dB and $\sim$ 13 dB OSNR for the same linewidth, respectively. The PCF combine with the RFP technique is slightly better than SIM-OFDM combine with the RFP technique [39, 44].

Figure 3.13 (b) shows the required OSNR for $1 \cdot 10^{-3}$ BER versus various linewidths of the lasers. It can be seen that both self-cancellation with the RFP technique and SIM-OFDM with the RFP show better than RFP only, especially when large linewidths are modeled. Note that the self-cancellation with the RFP can support laser linewidths over 1 MHz, but at the cost of spectral efficiency. Therefore, at 1 MHz laser linewidth, the SIM-OFDM is a possible choice for CO-OFDM system with 16-QAM and 1024-point IFFT/FFT [39, 44]. The disadvantage of SIM-OFDM can be handled using such algorithm in [39, 44].

Finally, the various phase noise suppression methods are compared by simulation. Significant improvements over RFP only arise for the process with reduced spectral efficiency. To efficiently cope with the loss in spectral efficiency, blind compensation is a good candidate to compensate for phase noise. But this technique requires high computational complexity, especially when large IFFT/FFT points and high-order modulation format and employed [59], so it is not suitable for practical use.

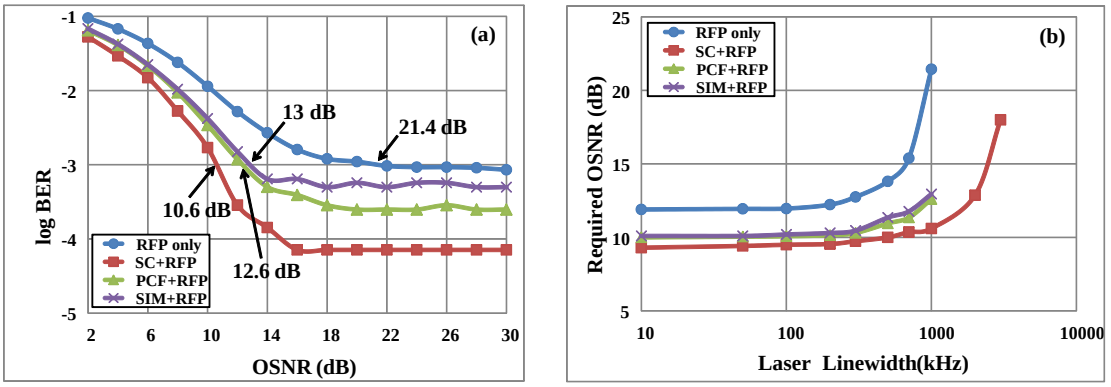

FIGURE 3.13: (a) BER performance for 1 MHz laser linewidth, (b) Required OSNR vs. laser linewidth for $BER = 10^{-3}$

Chapter 4

Implementation of CO-OFDM Systems

The focus of this chapter is to explain the experimental setup of the CO-OFDM system. The results revealed in this chapter have been processed offline, where the OFDM data are generated in MATLAB, and then uploaded into two field-programmable gate arrays (FPGAs): one for the I-component and the second for the Q-component. At the receiver and after detecting the signal with two pairs of photodiodes, the received data are stored in an oscilloscope and then processed offline by MATLAB.

Conventional OFDM and DFT-spread OFDM with different LPN mitigation techniques are being conducted in this chapter with different setup scenarios, e.g., optical back-to-back, over several spans, or with ECL and DFB lasers. A clear case could be made for the need to implement receiver online processing for the CO-OFDM system.

4.1 Transmission setup of the CO-OFDM system

Figure 4.1 presents the transmission setup of the CO-OFDM system considered in this chapter, consisting of three blocks: the transmitter block (presented in Subsection 4.1.1), the transmission link block (presented in Subsection 4.1.2), and the receiver block (presented in Subsection 4.1.3). The components in the transmitter and receiver blocks are unchanged for the experimental results revealed in this thesis; however, the transmission link block may be modified.

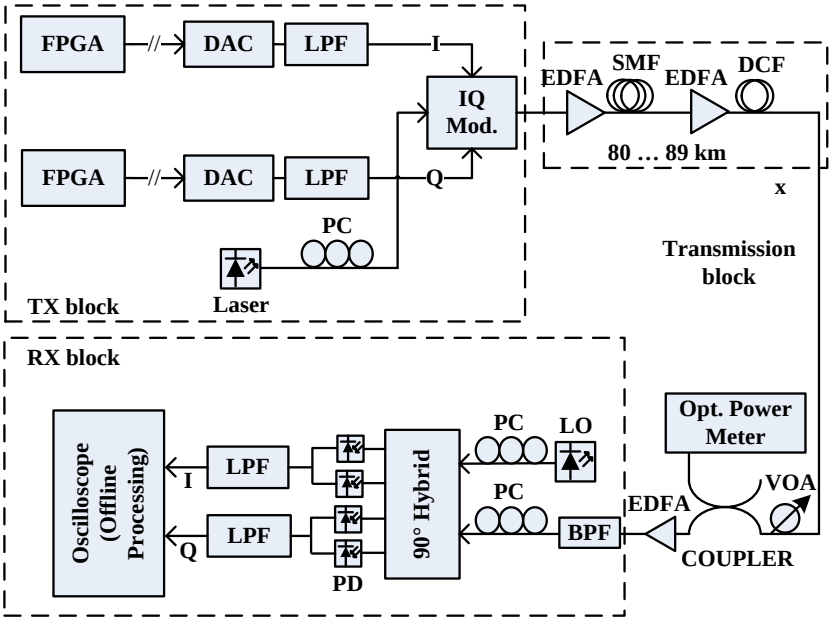

FIGURE 4.1: Experimental setup of the homodyne CO-OFDM system

4.1.1 Transmitter setup

Two FPGAs are employed to perform the DSP due to their flexibility and low cost compared to an application-specific integrated circuit (ASIC). Two Xilinx Virtex-4 (FX140) FPGAs with 24 RocketIO multi-gigabit transceivers (MGTs) are used for this thesis; each MGT has maximum line rate of 6.5 Gbps. Each FPGA is connected to a high-speed DAC. Two commercial DACs from Micram Vega with a 4:1 time multiplexer and 6-bit resolution are used in this thesis. Each DAC could run at speeds up to 28 GS/s. Twenty-four differential serial lines are employed to interface between the Virtex-4 FPGA and each Micram DAC. Due to the limited

speed of the MGT port of the available Virtex-4 FPGA, the DACs could be run at a maximum speed of 26 GS/s. Thus, each MGT is configured at the maximum line rate.

In the results presented in this thesis, the OFDM data are generated offline by mapping a $2^{17}-1$ PRBS sequence into quadrature phase-shift keying (QPSK), and then, different point values of the IFFT/FFT size with a certain value of cyclic prefix are considered to convert the frequency-domain signal into a time-domain signal. The time-domain signals are stored in LUTs on the FPGAs. The I-data that represent the real part are uploaded to one of the FPGAs, and the Q-data that represent the imaginary part are saved on the second FPGA.

The DACs are set to run at 15 GS/s with a data up-sampling factor of three; therefore, the actual sampling rate becomes 5 GS/s. After the DACs, two LPFs are equipped to remove the aliasing products of the DACs. Then, the analog signals are amplified and impressed onto the optical carrier by an Avanex SD50-DP Dual Parallel Modulator with a 25 dB optical extinction ratio. The modulator is based on two MZMs embedded in a Mach-Zehnder super-structure, where the optical signal is shifted by 90° on one of the MZMs to realize the I and Q components. Each MZM is designed to support a 50 Gb/s signal. This super-structure modulator could also be referred to as an IQ-MZM or DQPSK modulator.

4.1.2 Transmission Link

The transmission link consists of several spans, each span with either SSMF or nonzero dispersion-shifted fiber (NZDSF) and dispersion compensation fiber (DCF) modules that are inserted midway in double-stage EDFA. Section A.8 illustrates each span in detail. After the fiber link, the signal is fed into a variable optical attenuator (VOA) to adjust the receiver input power, followed by an optical preamplifier and an approximately 20 GHz-wide bandpass filter for noise filtering. Finally, the signal is fed into the coherent receiver.

4.1.3 Receiver setup

The coherent receiver consists of a conventional 90° hybrid mixer in which the received signal and LO are mixed together for coherent homodyne detection. The

polarizations of both the signal and LO are manually aligned by PCs. An alternative to the system setup shown in Figure 4.1 is to use the same laser at the transmitter and in the coherent receiver; this system setup will be indicated as self-homodyne CO-OFDM and is shown in Figure 4.2.

After the optical 90° hybrid, two differential photodiode pairs convert the signal from the optical domain to the electrical domain, where the output currents are converted to voltage signals by resistive loads [46]. Then, the electrical signal is sampled by a Tektronix TDS6804B oscilloscope at a sampling rate of 20 GS/s and at 8-bit resolution. Using the same oscilloscope, the data are stored and then processed offline by MATLAB.

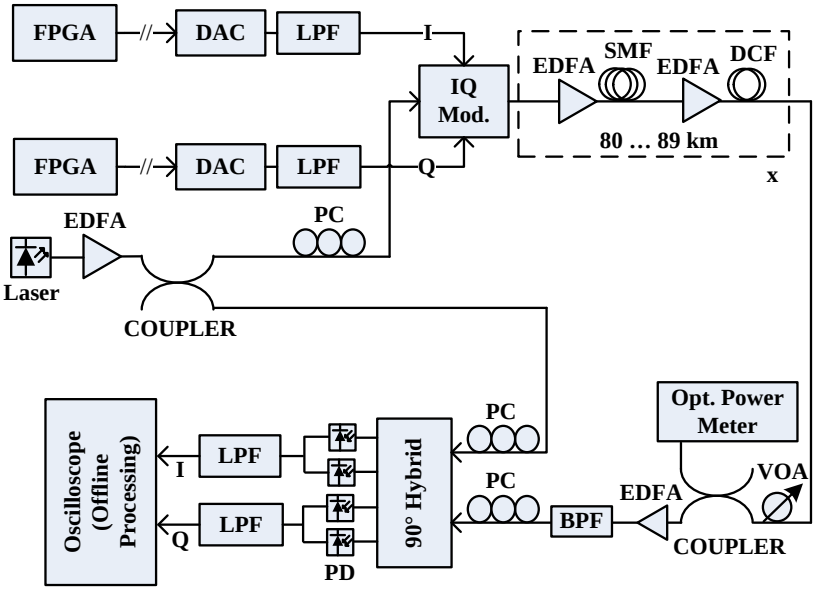

FIGURE 4.2: Experimental setup of the self-homodyne CO-OFDM system

4.2 Study of DFT-spread CO-OFDM systems

As many techniques have been investigated to mitigate the fiber nonlinearities by reducing the PAPR, the DFT spread is an attractive technique for long-haul CO-OFDM systems because of its higher tolerance for fiber nonlinearities [47]. This technique has been studied in simulation by several researchers; the experiments in this section have addressed the impact of LPN on the DFT-spread CO-OFDM system.

Therefore, the experiments presented in Section 4.2.3 are conducted to study the impact of LPN on DFT-spread OFDM [47]. Furthermore, two different LPN compensations are employed: CPE compensation and the non-iterative interpolation-based method. Moreover, a new spectral shaping to enhance the BER performance of the DSP-spread OFDM system is proposed and experimentally performed over a $\sim$ 347 km fiber link in Section 4.2.4.

The experiments carried out in this section are similar to those shown in Figure 4.2; the same commercial ECL is employed at the transmitter and as the LO in the coherent receiver.

4.2.1 Concept of DFT-Spread OFDM

DFT-spread OFDM adds only one block to the conventional OFDM. At the transmitter, the QPSK symbols are first separated into several subbands, where each subband sends to an L-point DFT, followed by an N-point IFFT that is applied to the combined subbands, as observed in Figure 4.3 (a) [47, 48]. This configuration reduces the PAPR because each subband produces a lower PAPR than when directly applying an IFFT. In the receiver, the inverse process is performed to recover the data by applying an N-point FFT followed by an L-point iDFT after separating the data into the same number of subbands that is used at the transmitter, as shown in Figure 4.3 (b).

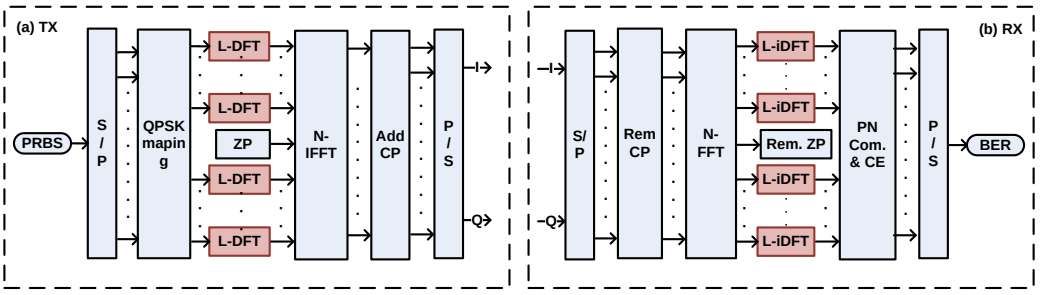

FIGURE 4.3: Schematic of a DFT-spread OFDM (a) at the transmitter, (b) in the receiver. The red boxes are removed for conventional OFDM. Legend: S/P=serial to parallel, ZP=zero padding, P/S=parallel to serial, Rem.=remove, PN Comp.=phase noise compensation, either by the CPE or non-iterative interpolation-based method

4.2.2 Concept of Non-iterative Interpolation Based LPN Mitigation

The non-iterative interpolation-based partial ICI mitigation is proposed in [49]. First, the CPE is estimated as in Equation 2.19 from Section 2.2.3. The use of this value is to only perform linear interpolation with the other estimation values of previous and next OFDM symbols.

Therefore, this estimated CPE value (CPE_i) will not be used for phase noise compensation as the case with CPE method in Section 2.2.4, but this value of each OFDM symbol is set to the value that occurs in the middle of the time-domain LPN effect of the same OFDM symbol. Then, the CPE estimation values are linearly interpolated between two adjacent OFDM symbols as illustrated in Figure 4.4 [49]. This indicates that the estimated CPE values are necessary to estimate the time-domain LPN effect between two adjacent OFDM symbols.

Finally, as in Equation 4.1, the received OFDM symbol after channel estimation and correction in the frequency-domain will be convolved by the conjugated spectral components of the time-domain LPN estimation i.e. the linear interpolation of the CPE estimation values of consecutive OFDM symbols. Taking FFT of the $L+1$ time-domain LPN estimation (after linear interpolation) results in Ps_{L+1}. The block diagram of the non-iterative interpolation-based method is shown in Figure 4.5.

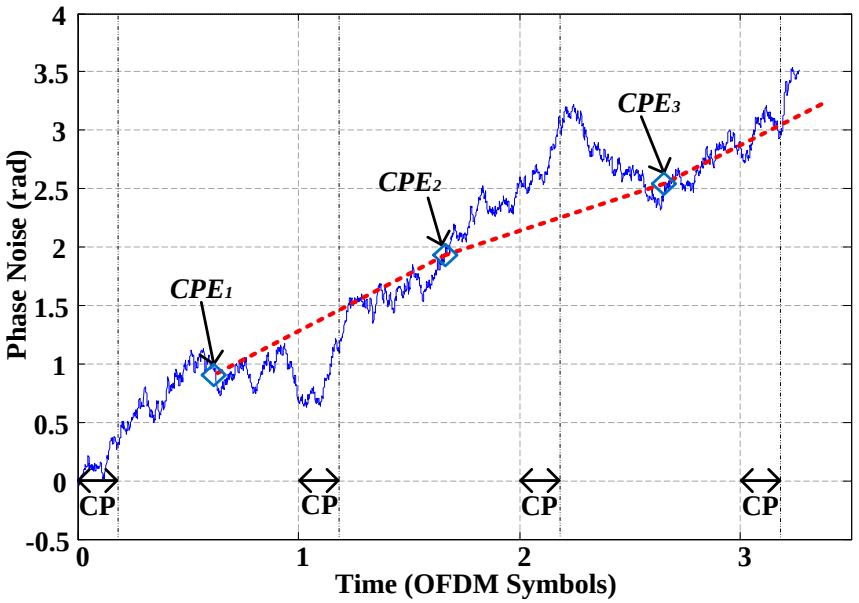

FIGURE 4.4: Example of the non-iterative interpolation-based method with linear interpolation over multiple CPE estimations

$$\hat{Y}_k^i = \sum_{l=-L/2}^{L/2} (conj(Ps_l) \cdot \grave{Y}_{k-l}^i)). \tag{4.1}$$

Equation 4.1 indicates that the received data can be convolved by the spectral components of the time domain phase noise estimation Ps_{L+1} where $\hat{Y}_k^i$ is the compensated OFDM-received data, $\grave{Y}_k^i$ is the OFDM-received data after channel correction and $L+1$ is the considered number of spectral components, i and k denote the OFDM symbol index and the OFDM subcarrier index, respectively. As shown in Figure 4.5, the Ps_{L+1} is (L+1)-number of spectral components which is considered for FFT size of phase noise estimation. YP^i is the received pilot subcarriers in the ith OFDM symbol.

In [49], the authors analyzed the complexity of the non-iterative interpolation-based phase noise mitigation method. They claimed that this method has significantly lower complexity compared to the iterative algorithms and similar complexity to the channel estimation and correction that applies to pilot symbols. However this method leads to a one-symbol delay because of the linear interpolation of CPE estimates applying to consecutive OFDM symbols.

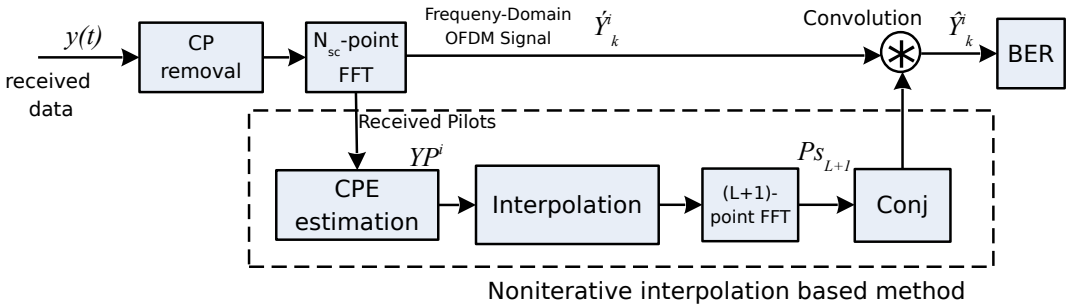

FIGURE 4.5: Block diagram of the non-iterative interpolation based method

4.2.3 Optical back-to-back Experiments on DFT-spread OFDM Systems

A $2^{17} - 1$ PRBS sequence is mapped into a QPSK to generate the OFDM signal. Then, either 608 or 1216 subcarriers are subdivided into several subbands. Each subband passes an L-point DFT. Finally, either a 1024- or 2048-point IFFT is employed on the subbands output data. The remaining subcarriers are padded with zeros to separate the baseband signal from the aliasing products [47]. Two additional training symbols are at the head of the transmission for timing synchronization and channel estimation.

4.2.3.1 Experimental Results

Figure 4.6 presents the BER performance of the system against RX input power for a 1024-point N-IFFT/FFT. Two scenarios are studied: a DFT-spread with 19 subbands, i.e., the L-DFT has 32 points, and the DFT-spread with 76 subbands, i.e., the L-DFT has eight points. Both scenarios based on the DFT-spread produce worse BER performance compared to the conventional CO-OFDM system with the 1024-point N-IFFT/FFT [47]. The LPN dominates for this setup, with a low sampling rate and a large number of IFFT/FFT points. The experimental results reveal that a DFT-spread CO-OFDM system is more prone to LPN than a conventional CO-OFDM system [47]. The LPN has a clear influence on the DFT-spread OFDM, where the neighboring subbands affect each other in a similar manner as the conventional OFDM subcarriers with narrow spacing [47, 48].

The 19-subband DFT-spread reports a better BER than the 76-subband DFT-spread. This result indicates that the impact of LPN is significantly increased

with an increasing number of subbands. Non-iterative interpolation-based LPN mitigation [49, 50] is employed for the DFT-spread CO-OFDM system to mitigate the LPN. The non-iterative interpolation-based method yields better BER performance than the conventional CPE for both the conventional CO-OFDM system and DFT-spread CO-OFDM system.

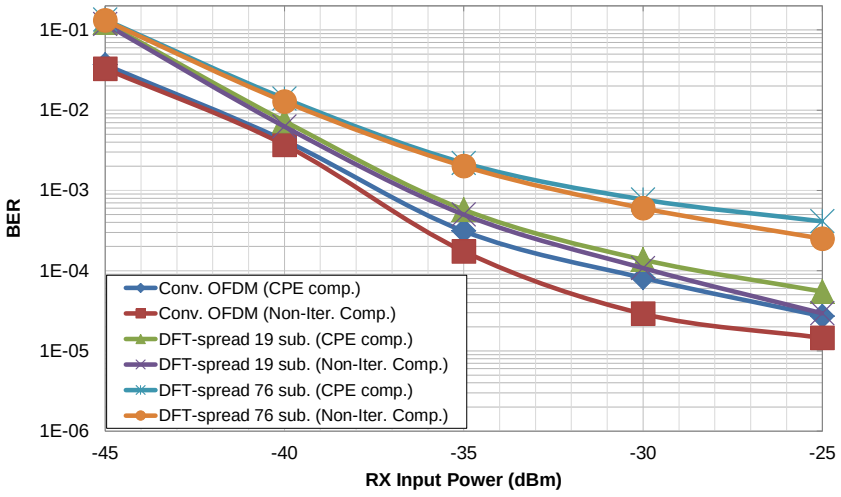

FIGURE 4.6: BER vs. RX input power of an N-IFFT/FFT with 1024 points

Figure 4.7 depicts the system BER vs. RX input power for a 2048-point N-IFFT/FFT. The results exhibit a similar behavior as those of the 1024-point N-IFFT/FFT. The lower number of subbands leads to a better BER, and the larger IFFT/FFT size leads to a higher penalty due to the LPN. This result can be observed by comparing Figures 4.6 and 4.7 for both the conventional CO-OFDM and DFT-spread OFDM systems [47].

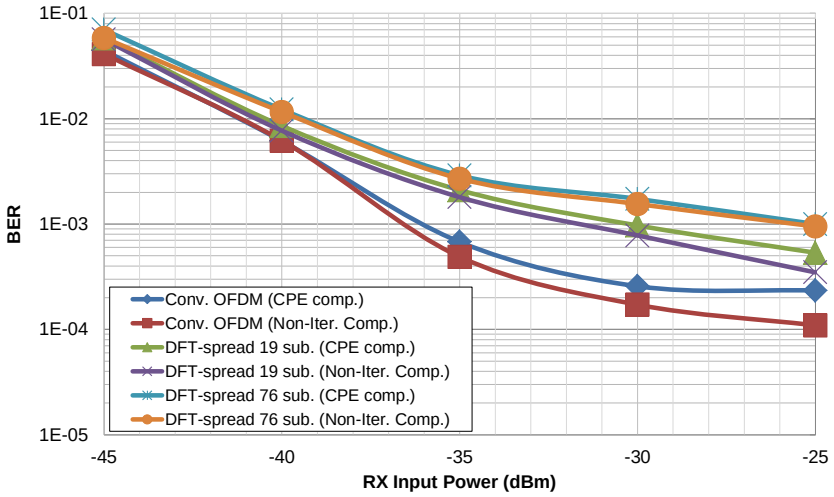

FIGURE 4.7: BER vs. RX input power of the 2048-point N-IFFT/FFT

4.2.4 Subband Spectral Shaping in DFT-spread CO-OFDM Systems

The recently proposed spectral shaping of DFT-spread OFDM (S-OFDM) has improved system performance in terms of the maximum transmission distance [51–53].

In [51], S-OFDM is presented by shaping the spectrum before applying the N-point IFFT, as observed in Figure 4.8 [51]. First stage in Figure 4.8 (A) is to divide the data into several subbands, each subband must have L-point subcarriers. Figure 4.8 (B) illustrates the process of L-point DFT for each subband, this stage is conventional DFT-spread OFDM. In Stage 2 Figure 4.8 (C), the spectrum is broadened by adding additional subcarriers at both sides of the OFDM spectrum to smooth the shape. This addition leads to an increase in the bandwidth of the S-OFDM. In comparison to the DFT-spread OFDM, the S-OFDM improves the maximum transmission distance by approximately 6.8% and 10.8% for a non-dispersion-managed (NDM) and dispersion-managed (DM) fiber link, respectively [51]. Reducing the PAPR increases the nonlinear tolerance more for DM fiber links than for NDM fiber links.

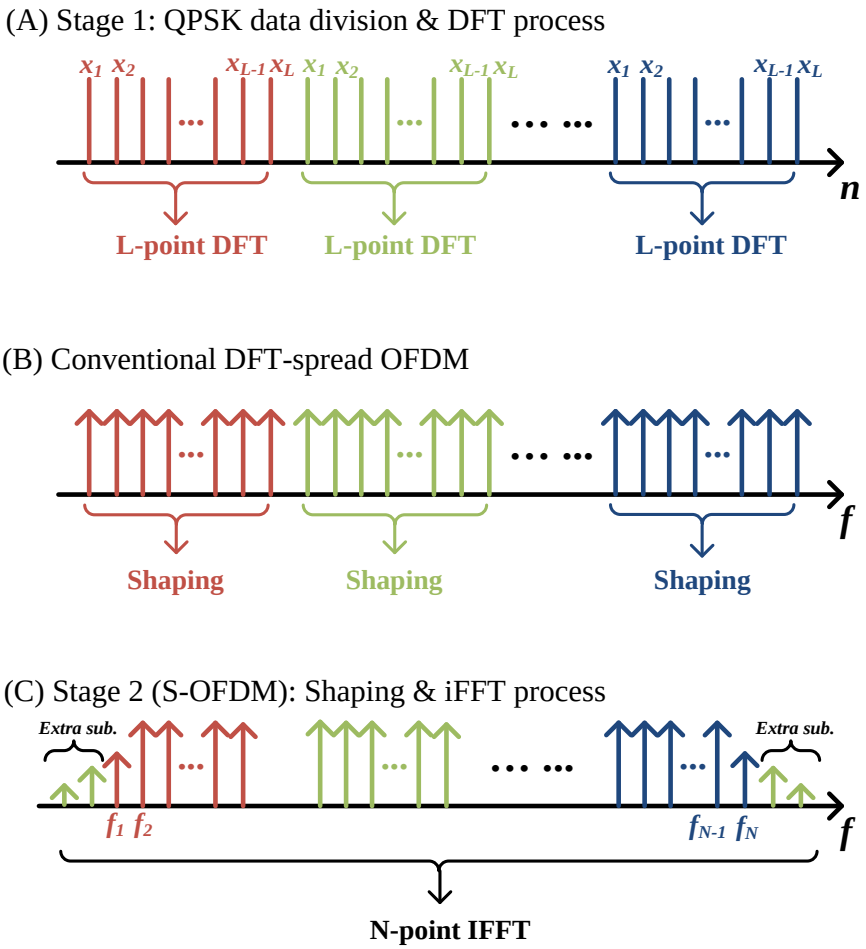

FIGURE 4.8: Spectral-shaping DFT-spread OFDM diagram (S-OFDM)

4.2.4.1 Modified Spectral-Shaping DFT-spread OFDM (MS-OFDM)

In this section, a new spectral-shaping method is presented in stage 2, as shown in Figure 4.9 (C). The first stage in Figure 4.9 (A) and (B) is same as for S-OFDM. The new spectral-shaping method is denoted as the modified spectral-shaping DFT-spread OFDM (MS-OFDM), where each subband of the DFT-spread OFDM is shaped instead of shaping and broadening the entire spectrum, as in S-OFDM [47, 51]. This approach reduces the ICI between the subbands and lowers the PAPR.

The same experiment setup of Section 4.2.3 is used here, with the exception that the QPSK data are subdivided into four subbands. Each subband passes a 128-point DFT and is shaped afterward [54]. Finally, a 1024-point IFFT is employed

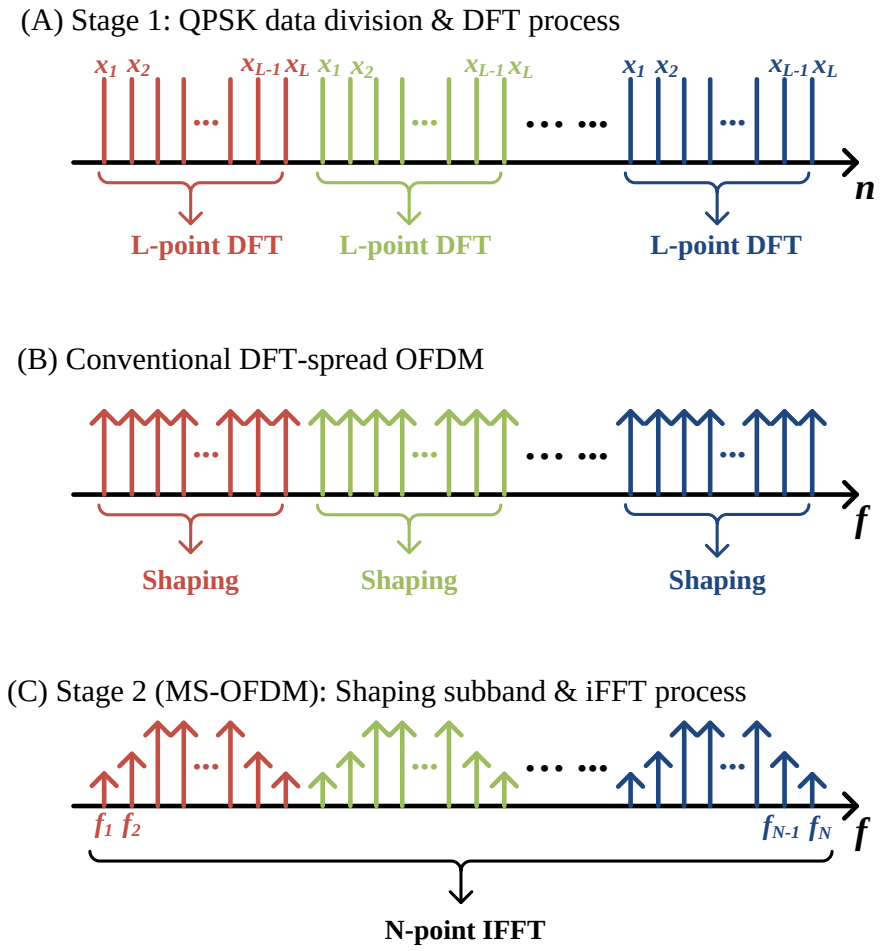

FIGURE 4.9: Modified spectral-shaping DFT-spread OFDM diagram

for the output data of the four subbands. The remaining subcarriers are padded with zeros to separate the baseband signal from the aliasing products. Two additional training symbols are at the head of the transmission for timing synchronization and channel estimation [54]. In this experiment, the transmission link consists of four spans (length 80,. . ., 89 km), each with EDFA and DCF. Then, the total fiber link is approximately 347 km (composed of 107 km of SSMF and 240 km of NZDSF).

4.2.4.2 Experimental Results

Figure 4.10 depicts the system BER against the RX input power after a distance of approximately 347 km at a launch power of −2 dBm. At a RX input power of 30

dBm, MS-OFDM yields $7.98 \cdot 10^{-5}$ and $6.55 \cdot 10^{-5}$ BERs for the CPE compensation and non-iterative interpolation-based method, respectively [54]. These results are better than the BER performance of the S-OFDM system, which yields BERs of $1.33 \cdot 10^{-4}$ and $1.02 \cdot 10^{-4}$ for the CPE compensation and non-iterative interpolation-based method, respectively. The non-iterative interpolation-based phase noise mitigation employed for the DFT-spread CO-OFDM system is clearly better than the conventional CPE compensation. For both LPN compensation methods, MS-OFDM exhibits distinctly better BER performance than S-OFDM.

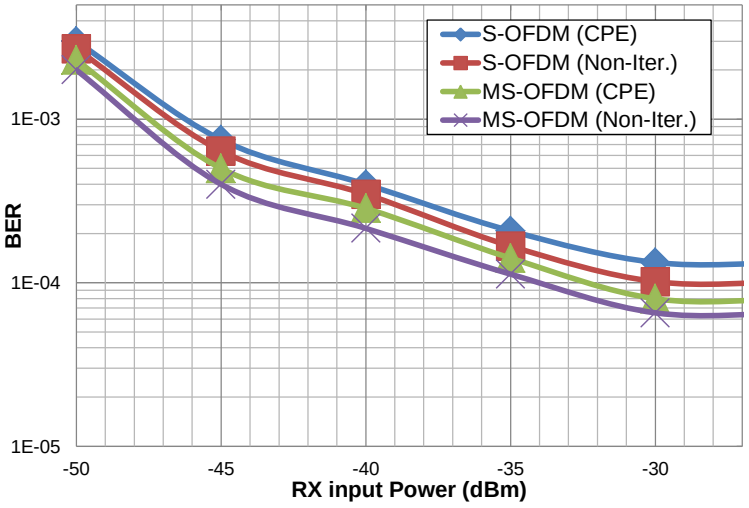

FIGURE 4.10: BER vs. RX input power for DFT-spread OFDM (S-OFDM and MS-OFDM) transmitted over approximately 347 km of fiber

4.3 Study of the Impact of LPN on CO-OFDM systems with a DFB Laser

CO-OFDM suffers from LPN, which strongly degrades the quality of the received signal [23, 24, 55]. This impact becomes more evident with longer OFDM symbols and lower sampling rates. The LPN can be mitigated with the RFP method [29], which is explained in Section 3.1.1.1. In most of the recent experiments with CO-OFDM systems [29, 41, 43, 56, 57], the RFP method is employed with ECL and a high sampling rate. The LPN can also be mitigated with the non-iterative interpolation-based method, in which the effect of ICI is partially compensated [50, 58]. To improve CO-OFDM systems that employ a low-cost DFB, we present a two-stage LPN mitigation consisting of RF-pilot mitigation in the time domain and a non-iterative interpolation-based method in the frequency domain.

4.3.1 Two-Stage LPN Mitigation Method

As shown in Figure 4.11, the first stage is the RFP method [29, 30], in which a pilot tone is placed in the middle of the transmitted OFDM signal. The pilot tone can be easily inserted by turning off the first OFDM subcarrier and to set a DC bias offset at the IQ-MZM. This pilot tone is affected by LPN in a similar way as the OFDM signal.

Therefore, the pilots are filtered out in a band-pass filter and are then used to compensate for the phase distortion of each OFDM symbol in the time domain. The RFP method requires a guard band to clearly filter the pilot tone. The second stage is the non-iterative interpolation-based method, where some pilots are placed near the DC subcarrier.

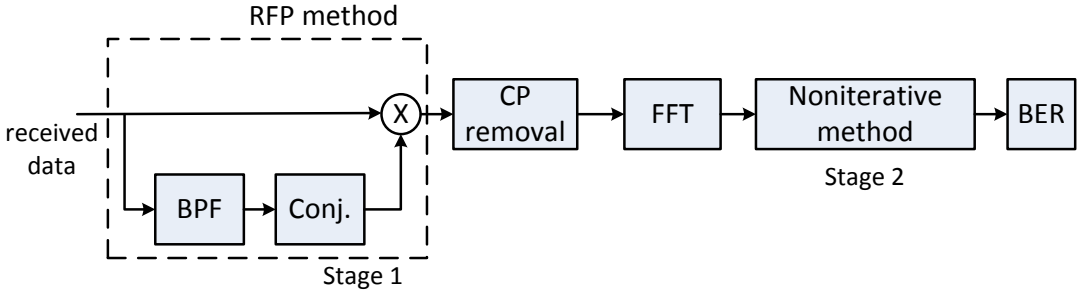

FIGURE 4.11: Block diagram of the Two-Stage LPN mitigation method

These pilots are generated to be stronger, i.e., to have twice the power, than the modulated data subcarriers used to enhance the estimation of phase differences. The extra power requires for pilots may has impact on PAPR, but the clipping method is considered before DACs. Figure 4.12 highlights the RFP and the stronger pilots in the received electrical-domain signal with a 1024-point IFFT/FFT, for a –30 dBm preamplier input power in the experimental setup.

Finally, the pilots are filtered out at the receiver in the frequency domain and compared to the stored original pilots to retrieve the phase difference. Using this phase difference, a non-iterative interpolation-based method (Section 4.2.2) [50, 58] is applied to mitigate the residual ICI impact.

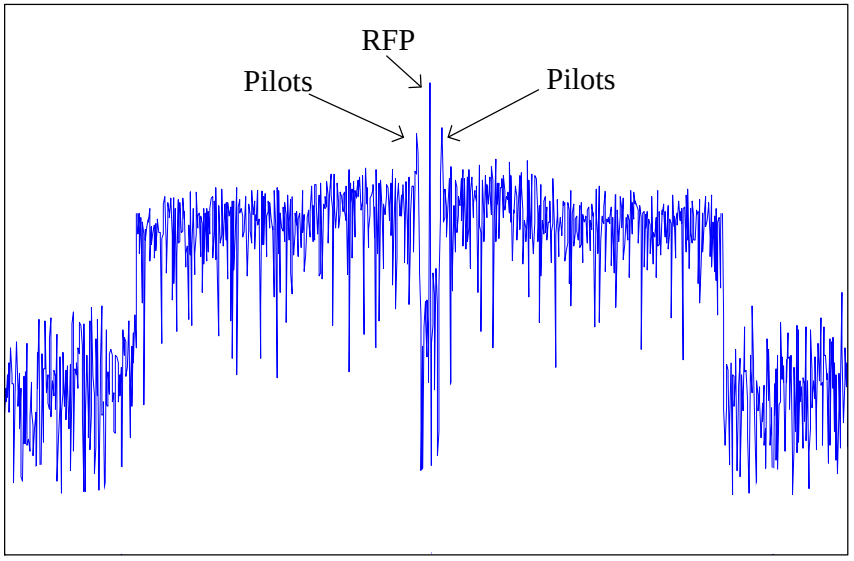

FIGURE 4.12: Received OFDM spectrum for a 1024-point IFFT/FFT at preamplifier input power of 25dBm

4.3.2 Homodyne Experiment with DFB Laser and ECL

The experimental setup of this section is as shown in Figure 4.1, where a low-cost DFB laser with a linewidth of approximately 1 MHz is set as a local oscillator and an ECL with a linewidth of approximately 150 kHz is used at the transmitter and vice verse. The transmission link of 1.6 km SSMF is considered. The OFDM signal is generated by mapping a $2^{17}-1$ PRBS sequence into QPSK and then transferring it to the time domain with an IFFT. Either 633 or 1,266 subcarriers are assigned to modulate the QPSK signal for the 1024- and 2048-point IFFT/FFTs, respectively. A guard band around the RFP is required to allow it to be clearly filtered at the receiver. Thus, a gap of 24 and 48 subcarriers is set around the RFP for the 1024- and 2048-point IFFT/FFTs, respectively [43]. The remaining subcarriers are padded with zeros to separate the baseband signal from the aliasing products. Two identical training symbols are inserted at the beginning of the OFDM frame to implement timing synchronization, channel estimation, and channel frequency offset [14].

Figures 4.13 and 4.14 present the BER vs. optical power at the preamplifier input for both the 1024- and 2048-point IFFT/FFTs. In Figure 4.13, the ECL is employed at the transmitter and the DFB laser is at the LO. In Figure 4.14, their locations are reversed.

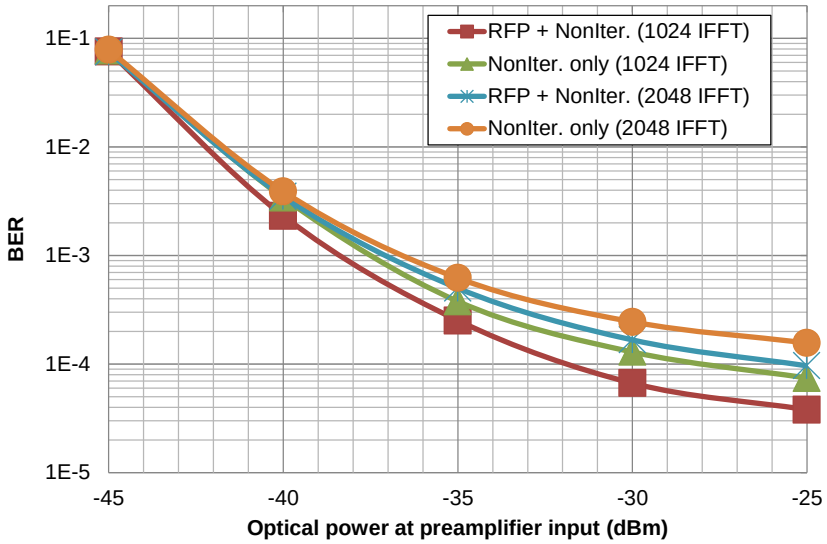

FIGURE 4.13: System BER vs. optical power at the preamplifier input when the DFB laser is set as the local oscillator

In Figure 4.13, at a preamplifier input power of -25 dBm, the best measured BERs for the 1024-point IFFT/FFT are $3.8 \cdot 10^{-5}$ and $7.45 \cdot 10^{-5}$ for the two-stage LPN mitigation and non-iterative interpolation-based methods, respectively. Thus, the two-stage method performs better compared to the non-iterative interpolation-based method only.

The 2048-point IFFT/FFT yields a BER of $9.64 \cdot 10^{-5}$ for the two-stage method and $1.57 \cdot 10^{-4}$ for the non-iterative interpolation-based method only. In general, the BER for the 1024-point IFFT/FFT is significantly lower than that for the 2048-point IFFT/FFT, likely because the larger IFFT/FFT size induces a higher penalty due to the impact of LPN. A similar BER performance can be observed in Figure 4.14. The BER performances of the LPN mitigation methods are similar if the signal is extremely noisy.

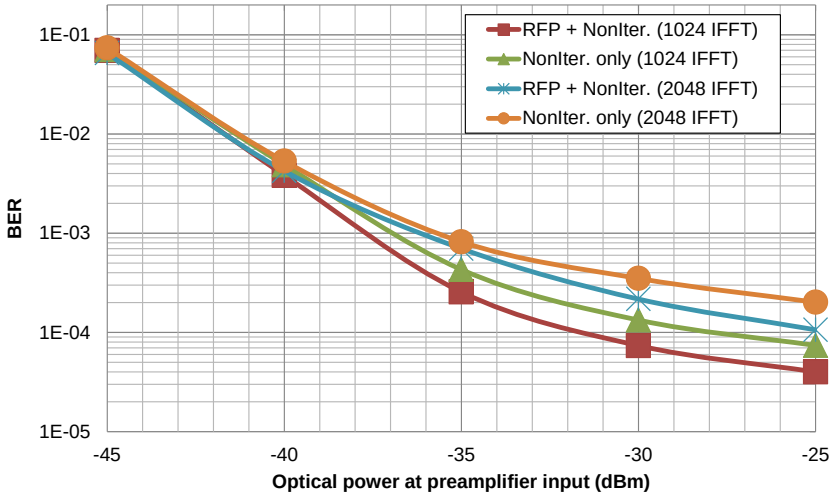

FIGURE 4.14: System BER vs. optical power at the preamplifier input when the DFB laser is set at the transmitter

4.3.3 Self-Homodyne Experiment with A DFB Laser

The self-homodyne experiment setup in Figure 4.2 is used, where the same DFB laser with a linewidth of approximately 1 MHz is employed at the transmitter and in the coherent receiver. Thus, the same frequency is used at the transmitter and the receiver, resulting in a zero CFO.

The transmission link of 1.6 km SSMF is implemented. The OFDM signal is generated by mapping a $2^{17}-1$ PRBS sequence into QPSK and then transferring it to the time domain with an IFFT. Either 633 or 1266 subcarriers are used to modulate the QPSK signal for the 1024- and 2048-point IFFT/FFTs, respectively. A guard band around the RFP is required to allow it to be clearly filtered at the receiver. Thus, a gap of 24 and 48 subcarriers is set around the RFP for the 1024- or 2048-point IFFT/FFTs, respectively [43]. The remaining subcarriers are padded with zeros to separate the baseband signal from the aliasing products. Two identical training symbols are inserted at the beginning of the OFDM frame to implement timing synchronization and channel estimation.

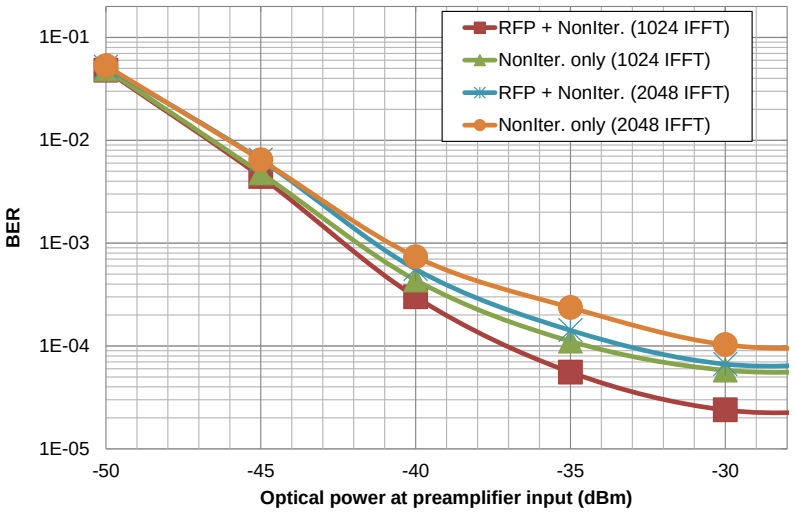

FIGURE 4.15: BER vs. optical power at the preamplifier input for the self-homodyne CO-OFDM system

Figure 4.15 presents the BER vs. optical power at the preamplifier input for the self-homodyne CO-OFDM system, where the same DFB laser is employed at the transmitter and in the coherent receiver. This configuration means that the same frequency is used at the transmitter and receiver, resulting in a zero

CFO. At the preamplifier input power of –30 dBm, the best measured BERs for the 1024-point IFFT/FFT are $2.38 \cdot 10^{-5}$ and $5.81 \cdot 10^{-5}$ for the two-stage LPN mitigation and non-iterative interpolation-based methods, respectively. The 2048-point IFFT/FFT yields BERs of $6.66 \cdot 10^{-5}$ for the two-stage method and $1.03 \cdot 10^{-4}$ for the non-iterative interpolation-based method only. These results support the conclusion that the two-stage method outperforms the non-iterative interpolation-based method. The direct comparison between the RFP and the two-stage method is not considered in the experiments because the RFP , that employed in both sides, simply mitigates both linear and non-linear phase noise which shows no significant beneficial improvements. In general this approved that the RFP is a promised method for phase noise compensation.

Chapter 5

Summary

This dissertation has presented the DSP algorithms that are required in homodyne CO-OFDM transmission: window synchronization, CFO correction, channel estimation and correction, LPN compensation, and fiber nonlinearity mitigation. The work is implemented in two stages: the simulation studies performed through VPITransmissionMaker with MATLAB and the experimental demonstration of the CO-OFDM system.

The simulation studies emphasize mitigating the effect of fiber nonlinearities, namely, SPM and XPM, and combating the LPN. The fiber nonlinearities have been mitigated by applying a combination of several techniques, such as the RF-pilot technique, PCF technique, and SIM-OFDM method.

As the PSR has a major influence on the system performance, the capability of the RFP mitigation technique with different PSR values has been reported to achieve the best PSR value. The simulation results indicate that the RF-pilot technique is a good candidate to compensate for XPM but does not effectively compensate for SPM. Thus, the RF-pilot combined with other techniques, such as the PCF and SIM-OFDM techniques, has successfully been extended to compensation for the XPM in long-haul CO-OFDM transmission. Although the RF-pilot technique combined with several scenarios of the PCF technique further improved the system Q-factor compared to using only the RF-pilot technique, the PCF technique suffers from low spectral efficiency as it uses only half of the subcarriers to carry data. One way to address this limitation of PCF is to apply a SIM-OFDM modulation method. SIM-OFDM modulation appends a new dimension to the QAM because

it uses the subcarrier index to convey information. Therefore, it has a higher spectral efficiency than the PCF technique.

The compensation for LPN is also a main topic of this dissertation. High-order modulation formats, such as 16-QAM, and large IFFT/FFT sizes, such as 1024-point, suffer more severely from LPN than the 4-QAM and 64-point IFFT/FFT formats, particularly if a cost-effective DFB laser with a large linewidth is employed. In the simulation of a CO-OFDM system with a 1024-point IFFT/FFT and a 16-QAM, ICI self-cancellation is examined in combination with the RF-pilot method to combat LPN. The combination of an RF-pilot technique with SIM-OFDM modulation is also explored to alleviate LPN. The simulation results indicated that self-cancellation combined with the RF-pilot techniques can support laser linewidths of over 1 MHz; however, such a combination is achieved at the expense of spectral efficiency because the self-cancellation technique reduces the spectral efficiency by a factor of two. SIM-OFDM combined with the RF-pilot technique exhibits a high tolerance to LPN with a better spectral efficiency. To efficiently cope with the loss in spectral efficiency, blind compensation is a perfect candidate to compensate for phase noise without pilots. This technique requires high computational complexity, especially when large IFFT/FFT points or high-order modulation format is employed [59]. Thus, SIM-OFDM with the RF-pilot technique is the recommended solution to enable the use of a DFB laser in a CO-OFDM system with a 1024-point IFFT/FFT and 16-QAM.

Finally, the experimental demonstration of the CO-OFDM system is carried out with an emphasis on the impact of LPN. First, self-homodyne and homodyne CO-OFDM systems with DFB lasers have been implemented with two-stage LPN mitigation. The experimental results of the 1024- and 2048-point IFFT/FFTs indicate the superiority of the two-stage mitigation method. Second, the experimental results examine this impact on the DFT-spread OFDM system. The results indicate that the DFT-spread OFDM system is more prone to LPN than the conventional CO-OFDM system. Additionally, a new spectral shaping method has been presented for a DFT-spread OFDM system. The experimental results over an approximately 347 km transmission exhibit an improvement in the BER when this new spectral shaping is employed.

Appendix A

Experimental Components

As mentioned in Section 4.1, the experimental setup consists of three blocks: the transmitter, transmission link, and receiver blocks. A list of the components used in the experimental setup are presented here with some details of their operation.

A.1 Xilinx Virtex-4 FPGAs

As shown in Figure A.1 (a), two Xilinx Virtex-4 (FX140) evaluation boards with 24 RocketIO MGTs are used to provide real-time transmission data; each MGT has a maximum line rate of 6.5 Gbps. The line rate of the MGT can be adjusted by changing the clock input to each block of MGTs.

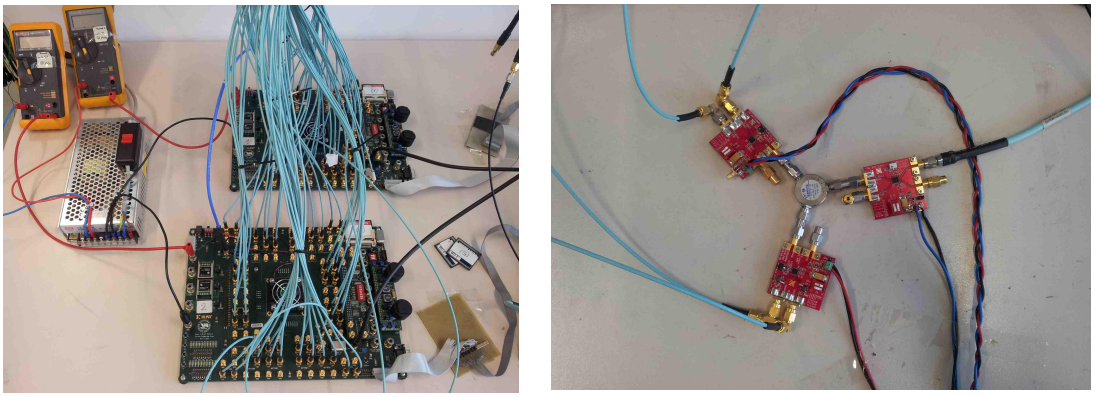

(a) (b)

FIGURE A.1: (a) Two Xilinx Virtex-4 FPGAs with a particular power supply, (b) three frequency dividers with a splitter

The power jacks of both FPGAs are unreliable in operation; therefore, the banana jacks with marks J27 and J33 are used. The current consumption of one FPGA depended on the operation speed of the transmitter system, e.g., when the system is running at 15 GSa/s, each FPGA draws approximately 5 Amp. Therefore, a special power supply is used to satisfy this requirement. The power supply can be observed in the left of Figure A.1 (a). The consumption of the current must be monitored using a current meter as it reflects the proper operation of the FPGAs. It is also important to monitor the fans of the FPGAs.

Each FPGA requires two clock signal lines to operate. These lines can be provided through frequency dividers with a splitter, as shown in Figure A.1 (b). The second FPGA board has a special VHDL code to shift the output signal. The requirement of this operation is to align the signals of the I and Q arms. Several dip switches (on the bottom left corner of the FPGA) are used to delay the signal of the second board by a certain number of bits (32, 16, 8, 4, 2, and 1 bit). This delay can align the signal within 1 bit. Two analog delay lines are used to obtain the fractional alignment that is placed before the attenuators.

A.2 MICRAM DACs

Two MICRAM DACs with VEGA evaluation boards are utilized to convert the signal into the analog domain, as shown in Figure A.2 (a). The maximum running speed of each DAC is 28 GSa/s with 6-bit resolution; each DAC contains a 4:1 multiplexer and 24 lanes. They are built to be compatible with the Xilinx Virtex-4 FX140 (more details in Section A.1) and the Xilinx Virtex-5.

As the maximum MGT speed of the available Xilinx Virtex-4 is 6.5 Gbps, and the maximum speed that can be reached for each DAC is 26 GSa/s. Each DAC needs the same frequency clock to be operated (i.e., 15 GHz for 15 GS/s). Two different values of voltage are required to operate the DACs: $\pm 3.3V$ and $\pm 5V$. The $-5V$ voltage must be turned on first, followed by the $-3V$ voltage, to avoid damaging the DAC. The opposite sequence must be followed when shutting down the DAC. As the FPGAs and DACs require a driving clock, the same function generator (Rohde & Schwarz SMP 04), shown in Figure A.2 A.2 (b), is used to provide a clock frequency for each component. This function generator generates a clock of 15 GHz, and then, this clock signal splits into two lines; the first line is

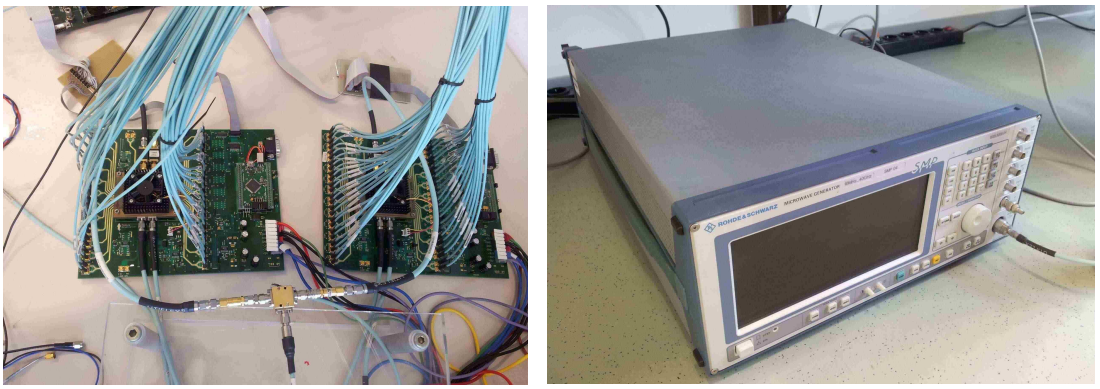

(a) (b)

FIGURE A.2: (a) Two MICRAM DACs with the VEGA evaluation board, (b) the Rohde Schwarz SMP-04 function generator

fed to the DACs after amplifying the signal because each DAC needs a signal with amplitude of 500 mV as a clock. The second line is fed to the frequency dividers to properly provide a clock frequency to each of the FPGAs, as shown in Figure A.1(b).

A.3 Avanex SD50-DP IQ-MZM

The Avanex SD50-DP Dual Parallel Modulator with a 25 dB optical extinction ratio has been employed in the experiments, as shown in Figure A.3. The modulator is based on two MZMs embedded in a Mach-Zehnder super-structure, where the optical signal is shifted by 90° on one of the MZMs to implement the I and Q components. Each MZM is designed to support a 50 Gb/s signal.

Two SHF 810 amplifiers are used to drive the RF ports of the MZMs; these amplifiers have a 29 dB amplification gain with an operating range of 40 kHz - 38 GHz. The typical driving voltage of the MZMs is 7 V ($2V_{pi}$), which reflects the need for such a high amplification gain. Three DC voltages adjust the bias V_{pi} of both the RF signals (MZ1 and MZ2) and the phase between them. A DC voltage supplier is built to adjust the voltage provided to each signal. The DC setup of this IQ-MZM is very critical; this piece of the IQ-MZM must be operated for at least one day to obtain a proper setting of the DC voltages. Therefore, the IQ-MZM is always operated with the input optical signal and DC voltages set up.

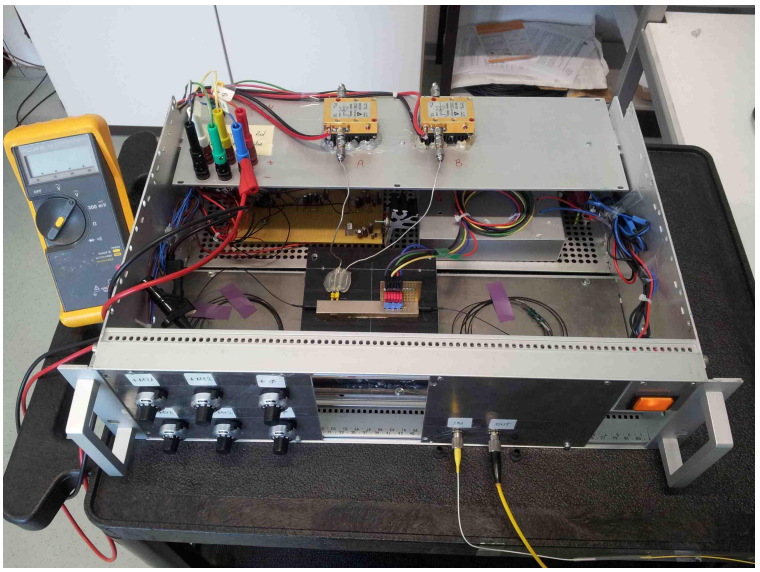

FIGURE A.3: Avanex SD50-DP IQ-MZM with amplifiers and DC voltage settings

A.4 ECL and DFB lasers

The HP 8168E commercial tunable ECL is employed in the experiments, as shown in Figure A.4 (a). This laser has a linewidth of approximately 150 kHz. In Figure A.4 (b), two DFB lasers from ORTEL with center wavelengths of 1545.32nm are built in the temperature and current-controlled machine. These lasers are given approximately a 1 MHz linewidth with some jitters. The first laser yields a higher jitter than the second laser.

(a) **(b)**

FIGURE A.4: (a) ECL tunable laser, (b) two DFB lasers

A.5 Polarization Controllers and 90° Optical Hyprid

Two PCs are used to manually align the received and local oscillator signals; these PCs are shown in Figure A.5 (a). The received and LO signals are mixed by a Celight 90° optical hybrid of model CL-QOH-90, which is shown in Figure A.5 (b).

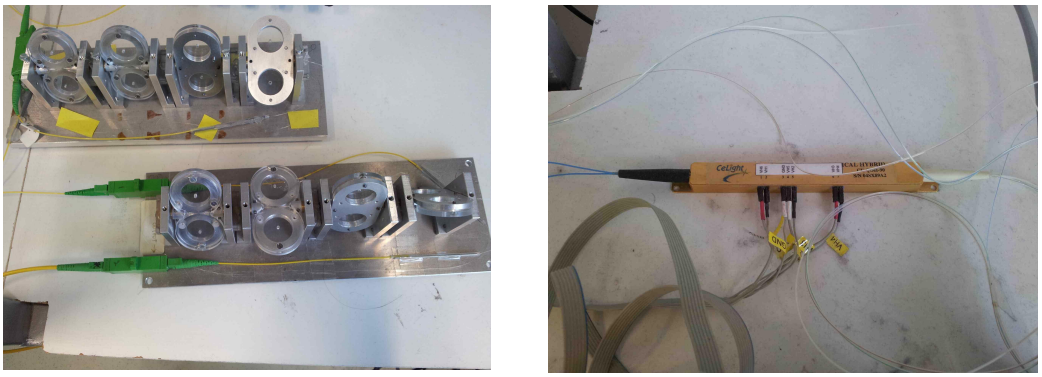

(a) (b)

FIGURE A.5: (a) Polarization Controller (b) Celight 90° Optical Hybrid

A.6 Photodiods and Oscilloscope

Two differential photodiode pairs convert the signal from the optical domain to the electrical domain, where the output currents are converted to voltage signals by resistive loads [46], as shown in Figure A.6 (a). These photodiodes come from Nortel (model PP-10G). They can operate for a 10 G system only. Then, the signal passes through two LPFs and is stored in the Tektronix TDS6804B oscilloscope with a sampling rate of 20 GS/s and an 8-bit resolution, as shown in Figure A.6 (b).

(a) (b)

FIGURE A.6: (a) Two differential photodiode pairs with resistive loads, (b) the Tektronix TDS6804B oscilloscope

A.7 High Speed Receiver

To cope with a high-speed system, i.e., beyond 10 G, a new receiver system is built and is shown in Figure A.7. This system consists of a polarization-diversified optical hybrid; the system can handle a maximum input optical power of 25 dBm and is a passive device; therefore, it does not need to any driving voltage, as with the Celight 90° optical hybrid.

Two 25 GHz balanced photo-detectors (model BPDV2020R) are set in the board. The maximum optical input power is 13 dBm with 50 Ohms. This configuration results in a 500 mV output voltage. The system has been tested with an input power of 10 dBm. The receiver has only been tested; it has not been put into operation for any results presented in this dissertation.

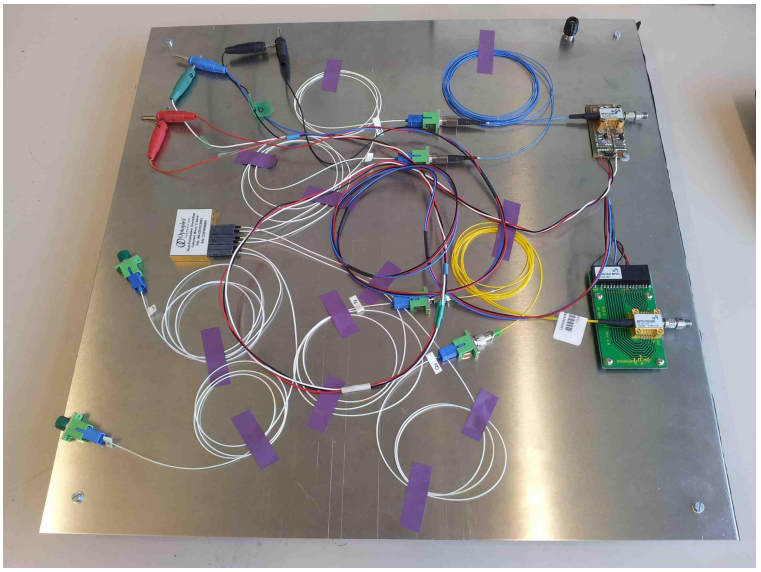

FIGURE A.7: Polarization-Diversified Optical Hybrid and Two Balanced Photo-detectors

A.8 Fiber Spans

Table A.1 provides the details of each available span. Each span includes a SSMF, NZDSF, or large effective area fiber (LEAF) with DCF modules that are inserted midway in a double-stage EDFA. The NZDSF is designed to solve the problem of dispersion-shifted fiber. Additionally, the nonlinear effects of this fiber are minimized [60].

Span 1	8.8km SSMF + 81.0km SSMF	= 89.8km
Span 2	8.0km SSMF + 80.0km NZDSF	= 88.0km
Span 3	8.0km SSMF + 80.0km NZDSF	= 88.0km
Span 4	81.5km NZDSF	= 81.5km
Span 5	20.0km LEAF + 63.0km SSMF	= 83.0km

TABLE A.1: Detailed information of each available spans

Bibliography

[1] Khaled Fazel and Stefan Kaiser. *Multi-carrier and spread spectrum systems: from OFDM and MC-CDMA to LTE and WiMAX*. Wiley, 2008.

[2] William Shieh and Ivan Djordjevic. *OFDM for optical communications*. Academic Press, 2009.

[3] Kazuro Kikuchi Masataka Nakazawa and Tetsuya Miyazaki. *High spectral density optical communication technologies*, volume 6. Springer, 2010.

[4] Lajos Hanzo, Matthias Münster, Byoung-Jo Choi, and Thomas Keller. *OFDM and MC-CDMA for broadband multi-user communications, WLANs and broadcasting*. John Wiley & Sons, 2003.

[5] S Weinstein and Paul Ebert. Data transmission by frequency-division multiplexing using the discrete fourier transform. *Communication Technology, IEEE Transactions on*, 19(5):628–634, 1971.

[6] Vinay K Ingle and John G Proakis. *Digital signal processing using MATLAB*. Thomson Engineering, 2011.

[7] Yan Tang. *High-speed Optical Transmission System Using Coherent Optical Orthogonal Frequency-division Multiplexing*. Ph.D thesis, University of Melbourne, Department of Electrical and Electronic Engineering, 2010.

[8] Qunbi Zhuge, Mohamed H. Morsy-Osman, and David V. Plant. Low overhead intra-symbol carrier phase recovery for reduced-guard-interval co-ofdm. *J. Lightwave Technol.*, 31(8):1158–1169, Apr 2013.

[9] Xiang Liu, S. Chandrasekhar, Benyuan Zhu, and David W. Peckham. Efficient digital coherent detection of a 1.2-tb/s 24-carrier no-guard-interval co-ofdm signal by simultaneously detecting multiple carriers per sampling. In *Optical*

Fiber Communication Conference, page OWO2. Optical Society of America, 2010.

[10] Akihide Sano, Eiichi Yamada, Hiroji Masuda, Etsushi Yamazaki, Takayuki Kobayashi, Eiji Yoshida, Yutaka Miyamoto, Riichi Kudo, Koichi Ishihara, and Yasushi Takatori. No-guard-interval coherent optical ofdm for 100-gb/s long-haul wdm transmission. *J. Lightwave Technol.*, 27(16):3705–3713, Aug 2009.

[11] Xiang Liu, S. Chandrasekhar, Benyuan Zhu, P.J. Winzer, A.H. Gnauck, and D.W. Peckham. 448-gb/s reduced-guard-interval co-ofdm transmission over 2000 km of ultra-large-area fiber and five 80-ghz-grid roadms. *Lightwave Technology, Journal of*, 29(4):483–490, 2011. ISSN 0733-8724.

[12] Xiang Liu, Peter Winzer, Chandrasekhar Sethumadhavan, Sebastian Randel, and Stephen Corteselli. Multiband dft-spread-ofdm equalizer with overlap-and-add dispersion compensation for low-overhead and low-complexity channel equalization. In *Optical Fiber Communication Conference*. Optical Society of America, 2013.

[13] Timothy M Schmidl and Donald C Cox. Robust frequency and timing synchronization for ofdm. *Communications, IEEE Transactions on*, 45(12):1613–1621, 1997.

[14] Paul H Moose. A technique for orthogonal frequency division multiplexing frequency offset correction. *Communications, IEEE Transactions on*, 42(10): 2908–2914, 1994.

[15] Xiang Liu and Fred Buchali. Intra-symbol frequency-domain averaging based channel estimation for coherent optical ofdm. *Optics express*, 16(26):21944–21957, 2008.

[16] Reinhold Noé. *Essentials of modern optical fiber communication*. Springer, 2010.

[17] W Shieh. Maximum-likelihood phase and channel estimation for coherent optical ofdm. *Photonics Technology Letters, IEEE*, 20(8):605–607, 2008.

[18] Songping Wu and Yeheskel Bar-Ness. A phase noise suppression algorithm for ofdm-based wlans. *Communications Letters, IEEE*, 6(12):535–537, 2002.

[19] Kidsanapong Puntsri, Omar Jan, Ali Mohammed Al-bermani, David Sandel, Christian Wördehoff, Saleh Hussin, Muhammad Fawad Panhwar, Ulrich Rückert, and Reinhold Noé. Pilot-aided CD and PN compensation simultaneously in CO-OFDM systems. In *The 10th Conference on Lasers and Electro-Optics Pacific Rim, and The 18th OptoElectronics and Communications Conference / Photonics in Switching 2013 (CLEO-PR&OECC/PS 2013)*, Kyoto, Japan, June 2013.

[20] Xingwen Yi, William Shieh, and Yan Tang. Phase estimation for coherent optical ofdm. *Photonics Technology Letters, IEEE*, 19(12):919–921, 2007.

[21] Seung Hee Han and Jae Hong Lee. An overview of peak-to-average power ratio reduction techniques for multicarrier transmission. *Wireless Communications, IEEE*, 12(2):56–65, 2005.

[22] Bernhard Goebel, STEPHAN Hellerbrand, Norman Haufe, and Norbert Hanik. Papr reduction techniques for coherent optical ofdm transmission. In *Transparent Optical Networks, 2009. ICTON'09. 11th International Conference on*, pages 1–4. IEEE, 2009.

[23] W Shieh, Hongchun Bao, Y Tang, et al. Coherent optical ofdm: theory and design. *Opt. Express*, 16(2):841–859, 2008.

[24] Jean Armstrong. Ofdm for optical communications. *Journal of lightwave technology*, 27(3):189–204, 2009.

[25] Brian S Krongold, Yan Tang, and William Shieh. Fiber nonlinearity mitigation by papr reduction in coherent optical ofdm systems via active constellation extension. In *Optical Communication, 2008. ECOC 2008. 34th European Conference on*, pages 1–2. IEEE, 2008.

[26] Moshe Nazarathy, Jacob Khurgin, Rakefet Weidenfeld, Yehuda Meiman, Pak Cho, Reinhold Noe, Isaac Shpantzer, and Vadim Karagodsky. Phased-array cancellation of nonlinear fwm in coherent ofdm dispersive multi-span links. *Optics express*, 16(20):15777–15810, 2008.

[27] Yan Tang, William Shieh, and Brian S Krongold. Fiber nonlinearity mitigation in 428-gb/s multiband coherent optical ofdm systems. In *Optical Fiber Communication Conference*. Optical Society of America, 2010.

[28] Omar Jan, M El-Darawy, K Puntsri, A Al-Bermani, and R Noé. Rf-pilot-based nonlinearity compensation in frequency domain for co-ofdm transmission. In *SPIE Photonics Europe*, pages 84340J–84340J. International Society for Optics and Photonics, 2012.

[29] Sander L Jansen, Itsuro Morita, Tim CW Schenk, Noriyuki Takeda, and Hideaki Tanaka. Coherent optical 25.8-gb/s ofdm transmission over 4160-km ssmf. *Journal of Lightwave Technology*, 26(1):6–15, 2008.

[30] Sebastian Randel, Susmita Adhikari, and Sander L Jansen. Analysis of rf-pilot-based phase noise compensation for coherent optical ofdm systems. *Photonics Technology Letters, IEEE*, 22(17):1288–1290, 2010.

[31] B Inan, S Randel, SL Jansen, A Lobato, S Adhikari, and N Hanik. Pilot-tone-based nonlinearity compensation for optical ofdm systems. In *Optical Communication (ECOC), 2010 36th European Conference and Exhibition on*, pages 1–3. IEEE, 2010.

[32] Omar Jan, Mohamed El-Darawy, Ali Al-Bermani, Kidsanapong Puntsri, and Reinhold Noé. Mitigation of fiber nonlinearities in co-ofdm systems. *ITG-Fachbericht-Photonische Netze*, 2012.

[33] Hongchun Bao, William Shieh, et al. Transmission simulation of coherent optical ofdm signals in wdm systems. *Opt. Express*, 15(8):4410–4418, 2007.

[34] Liang BY Du and Arthur J Lowery. Pilot-based xpm nonlinearity compensator for co-ofdm systems. *Optics express*, 19(26):B862–B867, 2011.

[35] Liang B Du and Arthur Lowery. Experimental demonstration of pilot-based xpm nonlinearity compensator for co-ofdm systems. In *European Conference and Exposition on Optical Communications*. Optical Society of America, 2011.

[36] O Jan, D Sandel, M El-Darawy, K Puntsri, A Al-Bermani, and R Noé. Fiber nonlinearity tolerance of sim-ofdm in co-ofdm transmission. In *Opto-Electronics and Communications Conference (OECC), 2012 17th*, pages 335–336. IEEE, 2012.

[37] Rami Abu-alhiga and Harald Haas. Subcarrier-index modulation ofdm. In *Personal, Indoor and Mobile Radio Communications, 2009 IEEE 20th International Symposium on*, pages 177–181. IEEE, 2009.

[38] Dobroslav Tsonev, Sinan Sinanovic, and Harald Haas. Enhanced subcarrier index modulation (sim) ofdm. In *GLOBECOM Workshops (GC Wkshps), 2011 IEEE*, pages 728–732. IEEE, 2011.

[39] Omar HA Jan, David Sandel, Kidsanapong Puntsri, Ali Al-Bermani, Mohamed El-Darawy, and Reinhold Noé. The robustness of subcarrier-index modulation in 16-qam co-ofdm system with 1024-point fft. *Optics express*, 20 (27):28963–28968, 2012.

[40] Abdullah Al Amin, Yue Xiao, and William Shieh. Performance evaluation of coded optical subcarrier index modulation ofdm format. In *Optical Fiber Communication Conference*. Optical Society of America, 2013.

[41] Beril Inan, Susmita Adhikari, Ozgur Karakaya, Peter Kainzmaier, Micheal Mocker, Heinrich von Kirchbauer, Norbert Hanik, Sander L Jansen, et al. Real-time 93.8-gb/s polarization-multiplexed ofdm transmitter with 1024-point ifft. *Opt. Express19 (26), B64–B68*, 2011.

[42] Rene Schmogrow, Marcus Winter, Bernd Nebendahl, David Hillerkuss, Joachim Meyer, Michael Dreschmann, Michael Huebner, Juergen Becker, Christian Koos, Wolfgang Freude, et al. 101.5 gbit/s real-time ofdm transmitter with 16qam modulated subcarriers. In *Proc. OFC*, 2011.

[43] Susmita Adhikari, Beril Inan, Ozgur Karakaya, Werner Rosenkranz, and Sander Jansen. Fft optimization for practical ofdm implementations. In *European Conference and Exposition on Optical Communications*. Optical Society of America, 2011.

[44] Omar Jan, David Sandel, Mohamed El-Darawy, Kidsanapong Puntsri, Ali Al-Bermani, and Reinhold Noé. Phase noise robustness of sim-ofdm in co-ofdm transmission. In *European Conference and Exhibition on Optical Communication*. Optical Society of America, 2012.

[45] Yuping Zhao and S-G Haggman. Intercarrier interference self-cancellation scheme for ofdm mobile communication systems. *Communications, IEEE Transactions on*, 49(7):1185–1191, 2001.

[46] Timo Pfau. *Development and Real-time Implementation of Digital Signal Processing Algorithms for Coherent Optical Receivers*. Ph.D thesis, University of Paderborn, Faculty for Electrical Engineering, Computer Science and Mathematics, 2009.

[47] Omar Jan, Ali Al-Bermani, Kidsanapong Puntsri, David Sandel, Christian Woerdehoff, Ulrich Rueckert, and Reinhold Noé. An experiment of coherent optical dft-spread ofdm with laser phase noise. In *Photonic Networks, 14. 2013 ITG Symposium. Proceedings*, pages 1–3. VDE, 2013.

[48] Yan Tang, William Shieh, and Brian S Krongold. Dft-spread ofdm for fiber nonlinearity mitigation. *Photonics Technology Letters, IEEE*, 22(16):1250–1252, 2010.

[49] Mohammad E Mousa-Pasandi and David V Plant. Noniterative interpolation-based partial phase noise ici mitigation for co-ofdm transport systems. *Photonics Technology Letters*, 23(21):1594–1596, 2011.

[50] Payam Rabiei, Won Namgoong, and Naofal Al-Dhahir. A non-iterative technique for phase noise ici mitigation in packet-based ofdm systems. *Signal Processing, IEEE Transactions on*, 58(11):5945–5950, 2010.

[51] Susmita Adhikari, Sander Jansen, Maxim Kuschnerov, Beril Inan, and Werner Rosenkranz. Analysis of spectrally shaped dfts-ofdm for fiber nonlinearity mitigation. In *European Conference and Exhibition on Optical Communication*. Optical Society of America, 2012.

[52] Susmita Adhikari, Sander Jansen, Maxim Kuschnerov, Beril Inan, Marc Bohn, and Werner Rosenkranz. Investigation of spectrally shaped dfts-ofdm for long haul transmission. *Optics express*, 20(26):B608–B614, 2012.

[53] Susmita Adhikari, Maxim Kuschnerov, Sander L Jansen, Adriana Lobato, Oscar Gaete, Beril Inan, and Werner Rosenkranz. Spectral shaping on dft-ofdm for higher transmission reach. In *Signal Processing in Photonic Communications*. Optical Society of America, 2012.

[54] Omar Jan, Kidsanapong Puntsri, David Sandel, Ali Mohammed Al-bermani, Christian Wördehoff, Ulrich Rückert, and Reinhold Noé. An experiment of subband spectral shaping in DFT-Spread CO-OFDM systems. In *The 10th Conference on Lasers and Electro-Optics Pacific Rim, and The 18th Opto-Electronics and Communications Conference / Photonics in Switching 2013 (CLEO-PR&OECC/PS 2013)*, Kyoto, Japan, June 2013.

[55] Moshe Nazarathy, R Weidenfeld, R Noe, Jacob Khurgin, Yehouda Meiman, Pak Cho, and Isaac Shpantzer. Recent advances in coherent optical ofdm

high-speed transmission. In *PhotonicsGlobal Singapore, 2008. IPGC 2008. IEEE*, pages 1–4. IEEE, 2008.

[56] Beril Inan, Ozgur Karakaya, Peter Kainzmaier, Susmita Adhikari, Stefano Calabro, Vincent Sleiffer, Norbert Hanik, and Sander L Jansen. Realization of a 23.9 gb/s real time optical-ofdm transmitter with a 1024 point ifft. In *Optical Fiber Communication Conference*. Optical Society of America, 2011.

[57] Dayou Qian, Ming-Fang Huang, Ezra Ip, Yue-Kai Huang, Yin Shao, Junqiang Hu, and Ting Wang. 101.7-tb/s (370× 294-gb/s) pdm-128qam-ofdm transmission over 3× 55-km ssmf using pilot-based phase noise mitigation. In *Optical Fiber Communication Conference*. Optical Society of America, 2011.

[58] Mohammad E Mousa-Pasandi, Qunbi Zhuge, Xian Xu, Mohamed M Osman, Ziad A El-Sahn, Mathieu Chagnon, and David V Plant. Experimental demonstration of non-iterative interpolation-based partial ici compensation in100g rgi-dp-co-ofdm transport systems. *Optics Express*, 20(14):14825–14832, 2012.

[59] Myung-Kyu Lee, Seung-Chan Lim, and Kyeongcheol Yang. Blind compensation for phase noise in ofdm systems over constant modulus modulation. *Communications, IEEE Transactions on*, 60(3):620–625, 2012.

[60] wikipedia. Non-zero dispersion-shifted fiber. URL http://en.wikipedia.org/wiki/Non-zero_dispersion-shifted_fiber.